A PARITY VIOLATION EXPERIMENT FOR UNDERGRADUATE LABORATORIES

By

Michael R. Ganger

A thesis submitted in partial fulfillment of the
requirements for the degree of

Bachelor of Science

Houghton College

May 2017

Signature of Author…………………………………………..………………………………….
Department of Physics
May 19, 2017

……………………………………………………………………………………………...
Dr. Mark Yuly
Professor of Physics
Research Supervisor

……………………………………………………………………………………………...
Dr. Brandon Hoffman
Associate Professor of Physics

A PARITY VIOLATION EXPERIMENT
FOR UNDERGRADUATE
LABORATORIES

By

Michael R. Ganger

Submitted to the Department of Physics
on May 19, 2017 in partial fulfillment of the
requirement for the degree of
Bachelor of Science

Abstract

The discovery of parity violation in weak interactions was a foundational discovery of the 20th century, first proposed by Lee and Yang in 1956 and experimentally verified by Wu in 1957. Lee and Yang also proposed a simpler experiment which does not require that the ^{60}Co source be polarized. Randomly oriented ^{60}Co beta decays to an excited state of ^{60}Ni, which then de-excites by emitting two gamma rays. Conservation of angular momentum ensures that the spins of all emitted particles are aligned. Therefore, when a gamma ray and a beta particle have antiparallel momenta they necessarily have opposite helicities. In the proposed experiment, these circularly polarized gamma rays are transmitted through a steel rod magnetized along the axis between two collinear detectors, a germanium detector for the gamma rays and a silicon detector for the beta particles. Due to the slight dependence of the Compton scattering cross-section on the relative orientations of the gamma rays and the electron spins in the magnet, a parity violating asymmetry may be observed by comparing beta particle and transmitted gamma ray coincidence count rates for opposite directions of magnetization. An experiment to observe effect this is currently being prepared at Houghton College using modern techniques suitable for an undergraduate laboratory.

Thesis Supervisor: Dr. Mark Yuly
Title: Professor of Physics

TABLE OF CONTENTS

TABLE OF FIGURES

Chapter 1

INTRODUCTION

1.1. Parity

Until the 1950's, it was assumed by theorists as well as experimentalists that the physical laws that govern the universe are independent of the coordinate system used. In other words, it was thought that the laws of physics worked identically in both right- and left-handed coordinate systems. Indeed, this was not an unreasonable assumption; in fact, most laws *are* independent of the handedness of the coordinate system. For example, the gravitational interaction of two massive bodies can be modeled using either convention of coordinate system, and both conventions will yield the same trajectories.

One way to switch between right- and left-handed coordinate systems is to perform a parity transformation. A parity transformation, denoted **P**, inverts all three spatial axes and changes the handedness of the coordinate system, as shown in Figure 1. A similar transformation which also switches the handedness is a mirror transformation, which inverts the sign of only one coordinate. A parity transformation is equivalent to a mirror transformation and a rotation; because the two are so closely related, it is often helpful to determine the effect of a parity transformation on a system by first considering the effect of a mirror transformation.

It can be said that a system invariant under a parity transformation exhibits a spatial symmetry. Noether's theorem [1] states that accompanying any symmetry of a system is a corresponding conserved quantity; the conserved quantity associated with parity symmetry is called *parity*. By this definition, systems which do not exhibit parity symmetry do not conserve parity; these systems are said to violate parity. The idea of parity originated with the development of Quantum Mechanics when Laporte [2] discovered that the wave function of an atom always switches from odd to even or vice versa when it emits or absorbs a photon; the even wave functions have parity +1 and the odd wave functions have parity -1 [3].

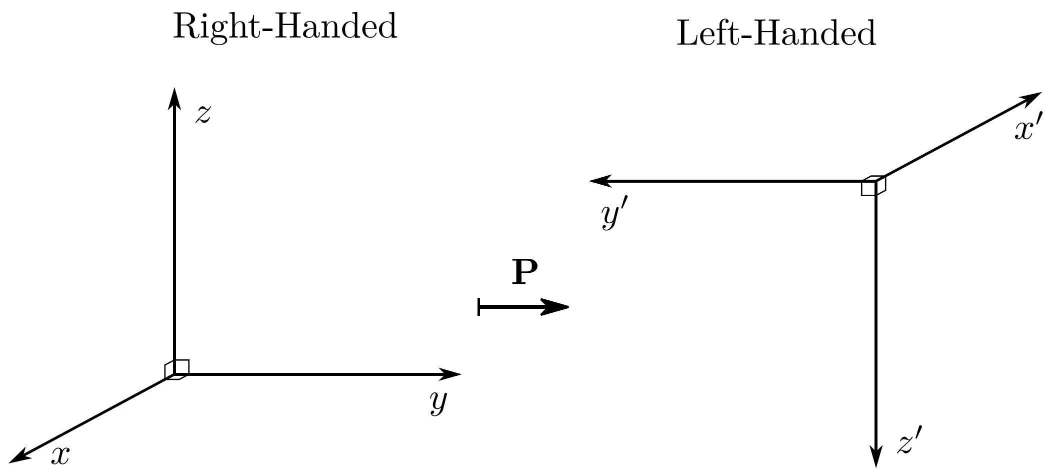

Figure 1. A parity transformation. A parity transformation, **P**, inverts all three spatial axes, resulting in a change from a right- to left-handed coordinate system.

Parity is known to be conserved in strong and electromagnetic interactions; this was confirmed by a number of experiments, the most accurate of which Lee and Yang took to be the measurement of the electric dipole of the neutron by Smith, et. al. [4, 5]. The experimentally determined upper limit on the dipole was less than 5×10^{-20} cm, which Lee and Yang found to place the upper limit on parity violation in strong and electromagnetic interactions at $\mathfrak{F}^2 < 3\times10^{-13}$, where $\mathfrak{F}^2$ is the fraction of atomic or nuclear states that possess a parity opposite to that which they would possess if they did not violate parity.

However, parity is not conserved in all interactions, although it was assumed to do so until the of the 1950's. In 1956, Lee and Yang [4] determined that there was no theoretical or experimental basis on which to assume that parity is conserved in weak interactions, and proposed a number of experiments which would test whether parity was conserved. The first experiment demonstrating parity violation in weak interactions was Wu [6] in 1957; this was a rather shocking discovery at the time because it showed that not only was parity violated in weak interactions, it was violated by a significant amount.

1.2. Original Research

1.2.1. Lee and Yang

The initial theory regarding the parity violation in weak interactions was developed by Lee and Yang in 1956 [4], who subsequently received a Nobel Prize in Physics (1957) for their work [7, 8]. The main importance of their work was to show that the conservation of parity could not be assumed *a priori*. However, they also proposed experimental tests that could be used to test conservation of parity. Their theoretical work was important in laying the groundwork for a number of ensuing experiments.

At the time, the idea that parity could be violated in weak interactions was considered outrageous. A number of physicists predicted that these would show that it was not. Richard Feynman even bet $50 that parity would not be violated [9]. However, the man responsible for introducing the idea of parity conservation in 1927, Eugene Wigner, suggested at the High Energy Physics Conference in Rochester that perhaps parity conservation did not hold for weak interactions [10].

Lee and Yang proposed four different experiments to test for the conservation of parity. The first experiment was to measure the asymmetry in the angular distribution of the emitted beta particles resulting from beta decay of a polarized nucleus. If an asymmetry was measured, it would indicate violation of parity; this is discussed in more detail in Section 1.3.1. The second experiment Lee and Yang proposed was to measure the circular polarization of a gamma ray in coincidence with a beta particle. For ^{60}Co, if an asymmetry in the right- and left-handed gamma rays emitted opposite a beta particle was detected, it would indicate an asymmetry in the helicity of the beta particles, implying the violation of parity. This is discussed in further detail in Section 1.3.2.

The third proposed experiment of Lee and Yang was to look at parity conservation in Λ^0 decay. This decay has the form

$$\pi^- + p \to \Lambda^0 + \theta^0, \qquad \Lambda^0 \to p + \pi^- . \tag{1}$$

The proposed experiment was to measure the quantity $R = \boldsymbol{p}_{out} \cdot (\boldsymbol{p}_{in} \times \boldsymbol{p}_{\Lambda^0})$, where $\boldsymbol{p}_{out}$, $\boldsymbol{p}_{in}$, and $\boldsymbol{p}_{\Lambda^0}$ are the momenta of the incoming π^-, the outgoing π^-, and the Λ^0 particle. By switching the handedness of the coordinate system, the sign of R should switch. If the magnitude of the two quantities is not identical, it indicates parity violation.

The fourth and final proposed test for parity violation that Lee and Yang proposed was to look at π decay of the form

$$\pi \rightarrow \mu + \nu_\mu, \qquad \mu \rightarrow e + \nu_e + \nu_\mu \,. \tag{2}$$

If an asymmetry in the distribution of the angle between $\boldsymbol{p}_\mu$ and $\boldsymbol{p}_e$ were observed, it would indicate parity violation in the μ decay. The argument for this is similar to that for β decay—if the π decay violates parity, the μ would be polarized along its direction of momentum, and if it also violates parity the emitted e would have an anisotropic angular distribution.

1.3. Past Experiments

1.3.1. Wu Experiment

The first experiment testing for parity violation was done by Wu in 1957 [6]. The experiment she performed used a polarized ^{60}Co source, which typically decays to an excited state of ^{60}Ni by emitting a beta particle and an antineutrino, and then the ^{60}Ni de-excited in two steps by emitting two gamma rays according to:

$$^{60}\mathrm{Co} \rightarrow {}^{60}\mathrm{Ni}^{*} + \beta^- + \bar{\nu}_e, \qquad {}^{60}\mathrm{Ni}^{*} \rightarrow {}^{60}\mathrm{Ni} + \gamma_1 + \gamma_2 \,. \tag{3}$$

This decay scheme may be seen in Figure 2.

The apparatus used by Wu, shown in Figure 3, measured the angular distribution of the emitted gamma rays from a polarized ^{60}Co source in order to monitor the ^{60}Co polarization. Because the decay of ^{60}Co to ^{60}Ni is a stretched state (that is, the angular momenta of the emitted particles add up to the difference in angular momentum between ^{60}Co and ^{60}Ni), the angular momentum of each emitted particle is in the same direction. Consequently, an observed anisotropy in the distribution of emitted γ from a polarized source indicates an anisotropy in the angular distribution of emitted beta particles, implying a preferred helicity for the beta particle in the initial decay (which violates parity conservation).

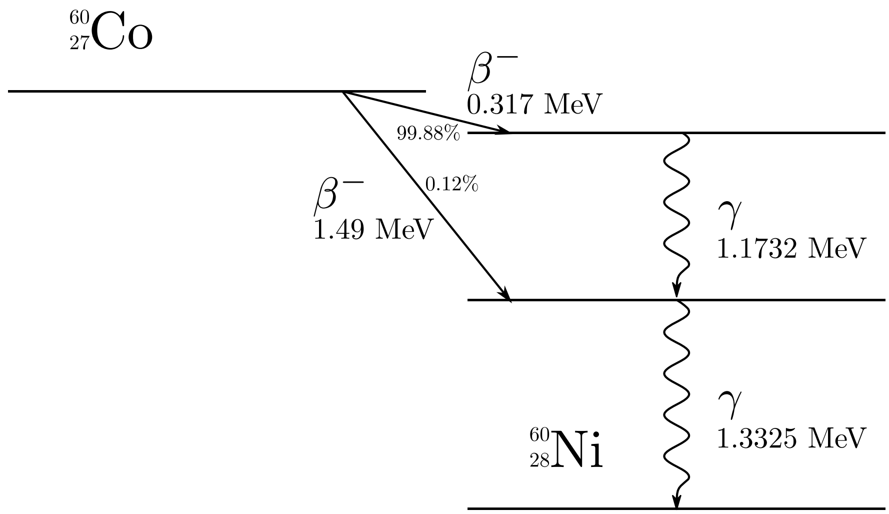

Figure 2. Decay of ^{60}Co to ^{60}Ni by emission of a beta particle and one or two gamma rays. Almost all decays (99.88%) result in two gamma rays, of energies 1.1732 MeV and 1.3325 MeV.

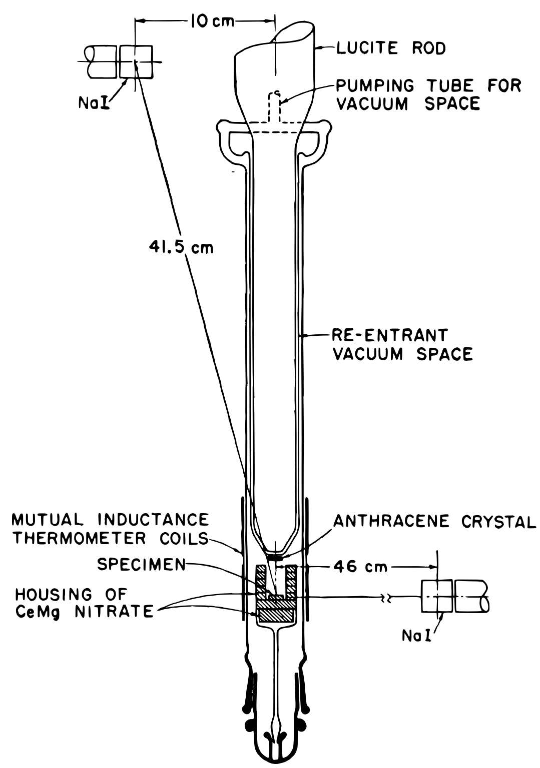

Figure 3. Schematic drawing of Wu apparatus. Electrons emitted from the beta decay collide with the anthracene crystal, producing a pulse of light which travels up the lucite rod and is detected and counted. The NaI detectors are used to quantify the polarity of the ^{60}Co specimen by detecting the fraction of of-axis gamma rays. Image taken from Wu [6].

Figure 4 shows the two scenarios which Wu's experiment was designed to test. The first scenario is when a polarized ^{60}Co nucleus emits a beta particle along its spin axis, and the second scenario is when it is emitted antiparallel to the spin axis. Parity conservation would imply that there would be an equal probability of both of these scenarios; in other words, that the distribution of beta particles from a polarized nucleus would be the same as under a mirror transformation. In order to test this, Wu's apparatus polarized the ^{60}Co nuclei in one direction, counted the number of beta particles emitted along that axis, and then inverted the polarization and counted the number of beta particles emitted antiparallel to the axis. The asymmetry of the measurement was then computed using the difference between the two emission rates.

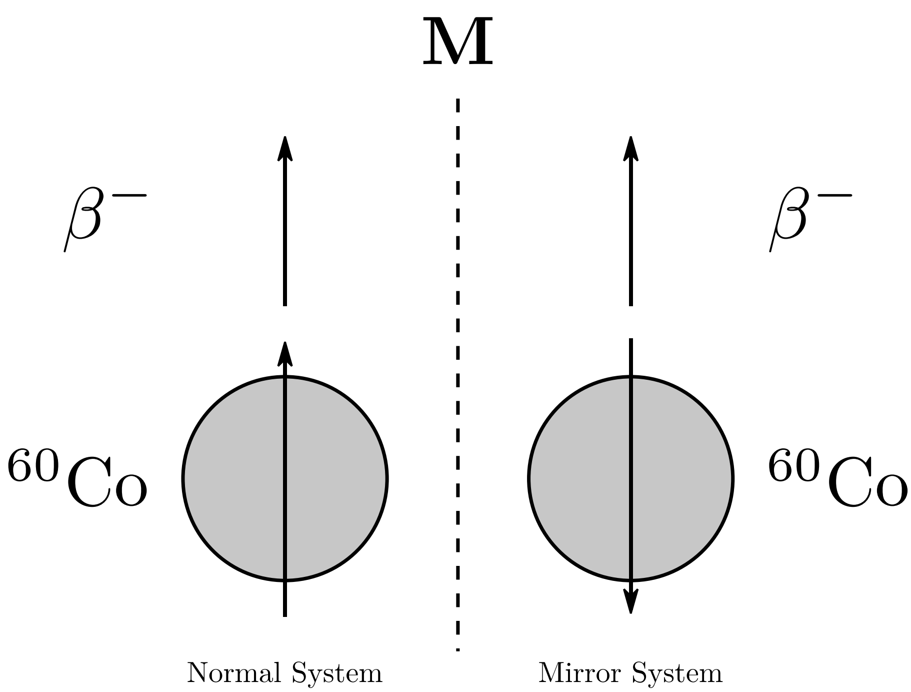

Figure 4. Comparison of ^{60}Co decay with its mirror image. In the normal system, the beta particle is emitted in the same direction as the spin of the ^{60}Co particle, but in the mirror system it is in the opposite direction.

The results of this experiment were surprising at the time as they not only demonstrated parity violation but also measured a large asymmetry of $\alpha = 0.4$, much greater than predicted by Lee and Yang. Up until this discovery, parity was assumed to be conserved in weak interactions by extrapolation; because strong and electromagnetic interactions were known to conserve parity, weak interactions were expected to do so as well. However, the discovery of parity violation indicated that at least one of the laws of physics is not independent of the handedness of the coordinate system.

1.3.2. Lundby Experiment

Soon after the results of the Wu experiment, Lundby et. al. [11] performed an experiment that used an unpolarized ^{60}Co source. The apparatus used in this experiment is shown in Figure 5. Photomultiplier tubes were set up collinear with the source and on opposite sides of a magnetized rod such that only beta particles and gamma rays with momenta in opposite directions weredetected, with the beta particle and gamma ray being detected by the lower and upper detectors, respectively. Only beta particles incident on the lower detector in coincidence with gamma rays on the upper detector were counted. The decay products of ^{60}Co, given in Eq. (3), are a beta particle, two gamma rays, and an antineutrino. Because the angular momenta of these must all be aligned, the helicities of the gamma particle and the beta particle must have opposite signs because their linear momenta are opposed. Thus, an observed asymmetry in the helicity of the detected gamma rays would indicate an asymmetry in the helicity of the beta particles, indicating that the decay violates parity conservation.

In order to observe an asymmetry in the helicities, a magnetized iron absorber was used. Due to a slight dependence in the Compton cross-section on the relative orientation of the angular momentum of the gamma ray and the aligned electron spin in the magnetization of the iron, there was a slight difference in attenuation as the gamma ray passed through the iron, resulting in slightly different count rates depending on the helicity of the emitted gamma rays. A slightly different count rate was detected with one magnet polarity than with the other, indicating that more gamma rays with one helicity were emitted than the opposite helicity. If parity was not violated, the count rates would have been equal between the two polarities; thus, an asymmetry in count rates indicated a violation of parity.

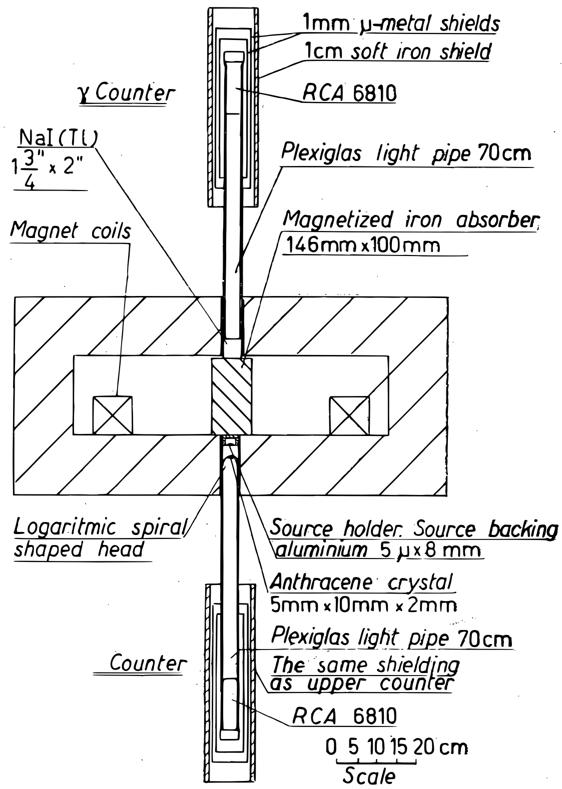

Figure 5. Diagram of the apparatus in Lundby's experiment. Beta particles emitted from the ^{60}Co source which strike the anthracene crystal produce light pulses that were detected by the lower photomultiplier tube. Gamma rays emitted from the source traversed the magnetized iron absorber and activated the upper photomultiplier tube. Only the gamma rays which were in coincidence with the beta particles were counted. Due to a slightly different attenuation based on the circular polarization of the gamma rays, switching the magnetization of the iron resulted in a different count rate if the gamma rays had a net circular polarization. Image taken from Lundby, et. al. [11].

1.3.3. Other Experiments

Following the experiments by Wu and Lundby, a number of other experiments were performed that verified their results. Goldhaber [12] found that bremsstrahlung produced by polarized beta particles is also circularly polarized. This was confirmed in a similar experiment performed by Schopper [13]. In an experiment performed by Garwin, et. al. [14], it was shown that parity asymmetry exists in μ^+ decay. This was confirmed by an experiment performed by Friedman, et. al. [15], which showed that the asymmetry also existed in $\pi^+ \to \mu^+ \to e^+$ decay. Another experiment, performed by Frauenfelder, et. al. [16], directly measured parity asymmetry by scattering the beta particles emitted from

^{60}Co decay, and found that the degree of asymmetry was related to the energy of the scattered beta particles.

Additionally, the verification of parity asymmetry led to the development of experiments to test for related symmetries. In a study by Jackson, et. al. [17], three experiments were proposed to test for beta decay symmetry with respect to time reversal, inspired by the proposal that parity asymmetry implies symmetry in charge conjugation, time reversal, or both.

As many of the early experiments demonstrating parity violation used ^{60}Co decay as the beta source, it was also important to establish that the beta-gamma correlation is isotropic; in other words, their directions are not statistically related. In a study by Daniel, et. al. [18], it was found that the beta-gamma directional correlation is essentially isotropic even accounting for small order effects. This result was obtained by fixing a source in a vacuum, with a scintillator to detect beta particles on one side of the source, and measuring the energy of the beta particles in coincidence with gamma rays at different angular distributions. Both ^{60}Co and ^{22}Na were used individually as sources in this experiment, and both an anthracene and a plastic scintillator were used to detect beta particles. The gamma rays were detected using a NaI crystal allowed to rotate about the source from 90° to 180° from the beta detector. A diagram of this experiment is shown in Figure 6. The results that the beta-gamma correlation was isotropic confirmed an earlier result found by Steffen [19], which used a similar setup but did not test for higher energies.

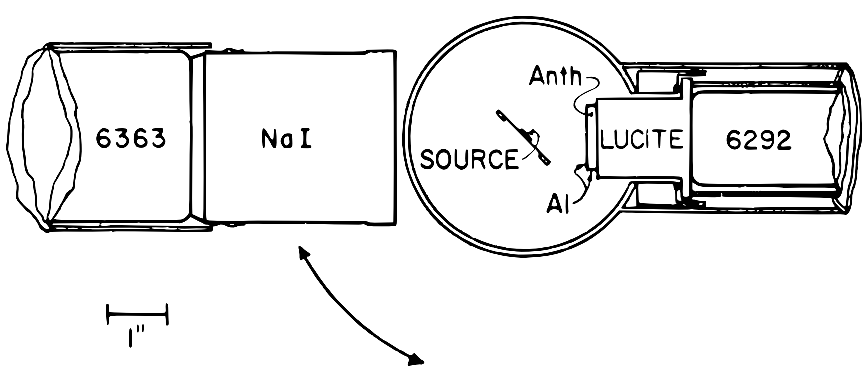

Figure 6. Apparatus used to measure beta-gamma correlation. The NaI detector is free to rotate around the source so as to measure the anisotropy of the beta decay source. Image taken from Daniel, et al. [18].

1.3.4. Neutrino Helicity

The products of ^{60}Co decay are two gamma rays, a beta particle, and an antineutrino. In order to determine the helicity of one of the particles, the helicity of the other two must be known. An experiment performed by Goldhaber [20] found that the neutrinos produced by the decay of ^{152m}Eu have only one helicity. It is important that the helicities of neutrinos be known because it allows for calculations involving the conservation of angular momentum in beta decay.

1.4. Proposed Experiment

1.4.1. Motivation for Experiment

The physical phenomenon that this experiment tests was discovered and verified about 60 years ago; as such, this experiment has little new scientific value beyond further verification of the original results. However, despite being a monumental discovery of modern physics, parity violation experiments are not part of the standard undergraduate nuclear physics curriculum. This is partially due to the expense and complexity of the original experiments that tested for parity violation. This thesis describes an experiment that uses modern technology and low-activity, exempt radioactive sources to demonstrate parity violation in an undergraduate setting. An important design consideration has been to use available and affordable equipment in a simple apparatus that can be replicated.

A search of the literature has only uncovered a single parity violation experiment for undergraduates [21]. The idea of this experiment is to measure the circular polarity of bremsstrahlung radiation produced by stopping polarized beta particles in a lead absorber. Because of parity violation, the beta particles from a decaying beta source will have a preferred helicity; if it is assumed that the gamma rays emitted from these beta particles when stopped have the same helicity, then the net helicity of the gamma rays may be used as a proxy for measuring the net helicity for the beta particles.

1.4.2. Basic Design

The experiment outlined in this thesis is similar to the one performed by Lundby, et. al. [11], as described in Section 1.3.2. It is a beta-gamma coincidence experiment that indirectly measures the polarization of gamma rays emitted during the decay of ^{60}Co. A silicon beta detector is placed near the source, and a germanium gamma detector is placed along the axis formed by the source and the beta detector. A magnetized iron rod was placed in between the source and the germanium detector. The iron rod is magnetized along the axis through the two detectors and the source; depending on the polarity of the magnetization, the transmission coefficient of the iron either increase or decreases due to a polarization-dependent difference in the Compton cross-section.

In general, the gamma rays emitted from an unpolarized ^{60}Co source will be unpolarized; that is, there will be equal numbers of right- and left-handed gamma rays. However, gamma rays detected in coincidence with beta particles at 180° will be circularly polarized. Because of parity violation, there is an anisotropic distribution of beta particles from a polarized ^{60}Co source, and as a consequence more beta particles from nuclei with one polarization will be detected than that of the opposite. The gamma rays detected in coincidence with beta particles are therefore polarized; thus, more gamma rays will be transmitted through the magnetized attenuator when it is magnetized in one direction along the axis than the opposite. A difference in the count rates between these opposing magnetizations therefore indicates a parity asymmetry in the beta decay.

1.4.3. Difference from Lundby Experiment

The experiment outlined in this paper, while similar to the experiment of Lundby, et al. [11], uses modern instruments allow for a simplified apparatus and circuit. In the experiment by Lundby, et al., photomultiplier tubes (RCA 6810) were used to detect both gamma rays and beta particles (using an anthracene crystal) from the decay of the ^{60}Co source; in the proposed experiment, silicon and germanium detectors are instead used to detect the beta particles and gamma rays, respectively. The advantage of using semiconductor detectors is that they provide significantly higher energy resolution over the original scintillators, decreasing the energy peak widths and increasing the ratio of real to accidental coincidences.

The electronics for proposed experiment replace the original analog electronics with a multiparameter acquisition system capable of reading both pulse heights and timing information on an event-by-event basis. An important benefit of this is that the definition of energy windows to determine count rates may be delayed until the experiment is complete. This eliminates the extra time required to collect data and determine suitable thresholds for both the gamma and the beta spectra before data collection, which is relatively significant when using a weak decay source. Furthermore, while this increases the overall complexity of the circuit, it reduces the amount of analog circuitry required to collect pulses.

Chapter 2

THEORY

2.1. Introduction

In this chapter, the theory important to understanding the experiment presented in this thesis is discussed. First, the operation of a parity transformation is defined, as well as what is meant by parity conservation. Then, ^{60}Co decay is considered, with particular attention to the angular momenta of the decay products and how the handedness of the emitted gamma rays relates to the parity asymmetry of the decay. After that, the attenuation of the circularly polarized gamma rays through a ferromagnetic material is calculated, and it is shown that a magnetized ferromagnetic material may be used to differentiate left- and right-handed gamma rays. The time required for obtaining a measurement is then estimated. Finally, the possible effect of ferromagnetic hysteresis is considered.

2.2. Parity Transformation and Conservation

A parity transformation usually refers to an inversion of all three spatial coordinates, applying the operation

$$\mathbf{P} : \begin{pmatrix} x \\ y \\ z \end{pmatrix} \mapsto \begin{pmatrix} -x \\ -y \\ -z \end{pmatrix} . \qquad (4)$$

If a system is invariant under parity inversion, it exhibits parity symmetry. By Noether's theorem [1], this means that there is a corresponding quantity that is conserved in the system. Thus, if a system is invariant under parity inversion, it must conserve a quantity known as "parity".

In quantum mechanics, the quantity "parity" corresponds to the evenness or oddness of the wavefunction describing the system. Thus, if a system with the wavefunction Ψ has even parity, then

$$\Psi(x, y, z, t) = \Psi(-x, -y, -z, t) \; , \qquad (5)$$

or, if it has odd parity,

$$\Psi(x, y, z, t) = -\Psi(-x, -y, -z, t). \tag{6}$$

Parity conservation, then, is the invariance of the evenness or oddness of the wavefunction under transformation. For example, if parity is conserved in a certain decay, the wavefunctions describing the system before and after the decay will exhibit the same parity.

In effect, what parity conservation means is that measurements taken of a system and its parity-transformed inverse will be identical if the system conserves parity. Conversely, if it can be shown that a certain measurement of a system changes when the system is transformed, this indicates that the system does not conserve parity.

2.3. Parity Violation in Weak Interactions

2.3.1. ^{60}Co Decay

The decay of ^{60}Co is one example of an interaction that does not conserve parity. Because it decays by emitting a beta particle, it is the result of weak interactions in the nucleus. Due to parity violation, more left-handed beta particles are emitted than the right-handed. For reasons that will be discussed below, conservation of angular momentum therefore requires that a polarized nucleus emits more beta particles antiparallel to its spin axis rather than parallel. Furthermore, the gamma rays emitted in the opposite direction to the beta particle are circularly polarized, with angular momentum in the same direction as the beta particle spin. Thus, if it can be shown that the numbers of left- and right-handed gamma rays are unequal, it can be shown that ^{60}Co decay violates parity violation.

The beta decay of ^{60}Co follows the reaction

$$^{60}\mathrm{Co} \rightarrow \beta^- + \bar{\nu_e} + {}^{60}\mathrm{Ni}^*\,, \tag{7}$$

$$^{60}\mathrm{Ni}^* \rightarrow \gamma_1 + \gamma_2 + {}^{60}\mathrm{Ni}\,. \tag{8}$$

The energy level diagram for this reaction is shown in Figure 2. A majority of the decays will beta decay to the second excited state of ^{60}Ni and subsequently decay to the ground state by releasing two gamma rays; a small fraction of the ^{60}Co decays will decay directly to the first excited state of ^{60}Ni, which then emits only one gamma ray as it de-excites to the ground state. As can be seen in Figure 2, the gamma rays released in the de-excitation have slightly different energies; this creates distinct peaks in the gamma spectroscopy of the nucleus. Unlike the gamma rays, however, the spectrum of the beta particles exhibits a distribution energies.

An important aspect of ^{60}Co decay is that the conservation of angular momentum only allows a single configuration of the angular momenta of all the decay products. Figure 7 shows the addition of the z-component of the angular momentum of each particle in the decay of ^{60}Co to ^{60}Ni, in units of $\hbar$. This is a stretched state, which means that the z-component of angular momentum held by each particle is the maximum value which it can have. In other words, the z-components of angular momenta for each particle can only add in one way to get the original angular momentum of the ^{60}Co nucleus.

This is an important aspect of ^{60}Co decay which is utilized for this experiment. When a gamma ray and beta particle are emitted in opposite directions, the z-components of their angular momenta must be in the same direction. This means that a right-handed beta particle is emitted directly opposite a left-handed gamma ray, and a left-handed beta particle opposite a right-handed gamma ray. Consequently, the asymmetry of right- and left-handed beta particles is the same as the asymmetry of left- and right-handed gamma rays emitted in coincidence with a beta particle traveling in the opposite direction; thus, the measurement of an asymmetry of left- and right-handed gamma rays emitted opposite a beta particle indicates an asymmetry of right- and left-handed beta particles.

One thing to note about Figure 7 is that the gamma rays have a z-component of angular momenta of $2\hbar$. Photons carry $\hbar$ of spin angular momentum in the z-direction because they are spin-1 particles. In order for the gamma ray to carry $2\hbar$ of angular momentum, it carries both orbital angular momentum as well as its spin angular momentum. Because of this, the decay is a stretched state; in other words, the angular momentum corresponding to each particle shown in Figure 7 is the only allowed value for that particle when the decay of ^{60}Co emits two gamma rays.

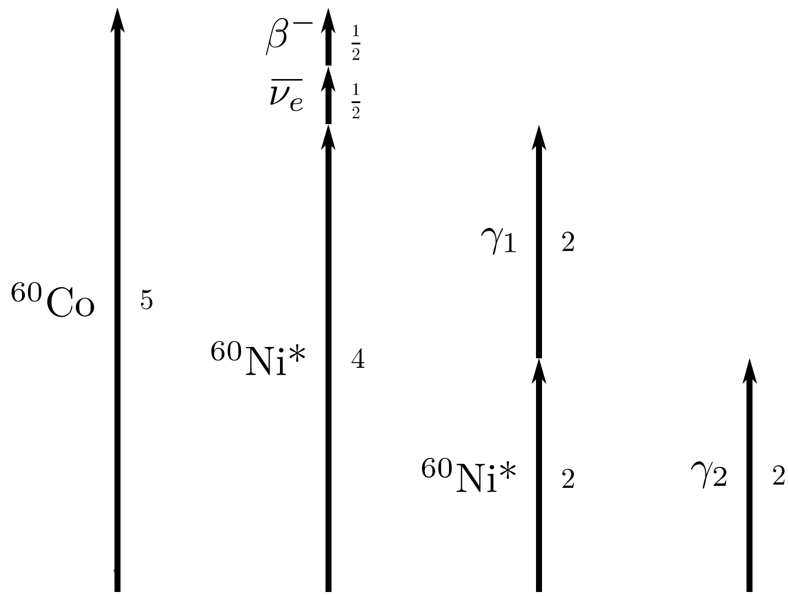

Figure 7. Conservation of z-component of angular momentum in decay of ^{60}Co. The numbers on the right side of each arrow correspond to the amount of angular momentum carried by that particle, in units of $\hbar$.

2.3.2. Collinear Momentum of Beta Particles and Gamma Rays

Figure 7 shows that the angular momenta of all the decay products are aligned in the most probable decay scheme. However, the linear momenta of the particles may be aligned in different orientations. In this experiment, only the scenario where the gamma ray and the beta particle have oppositely-directed momenta is measured. This is done by placing the gamma and beta detectors on opposite sides of ^{60}Co source and only counting gamma rays which are detected in coincidence with a beta particle. By only detecting these gamma rays, it is ensured that the gamma rays are circularly polarized.

In Figure 8, a diagram showing the basic principle of the experiment may be seen. Beta particles emitted from the decay of the unpolarized ^{60}Co source are detected by a silicon detector above the source, and gamma rays emitted in coincidence with the beta particle are detected by a germanium detector below the source and magnet. The magnet acts as a filter for the circularly polarized gamma rays, having a slightly different attenuation for left- and right-handed circularly polarized gamma rays, depending on the polarity of the magnetic field. This is shown in Figure 9. By switching the direction of the magnetic field, the presence of a difference in the count rates for left- and right-handed gamma rays may be observed.

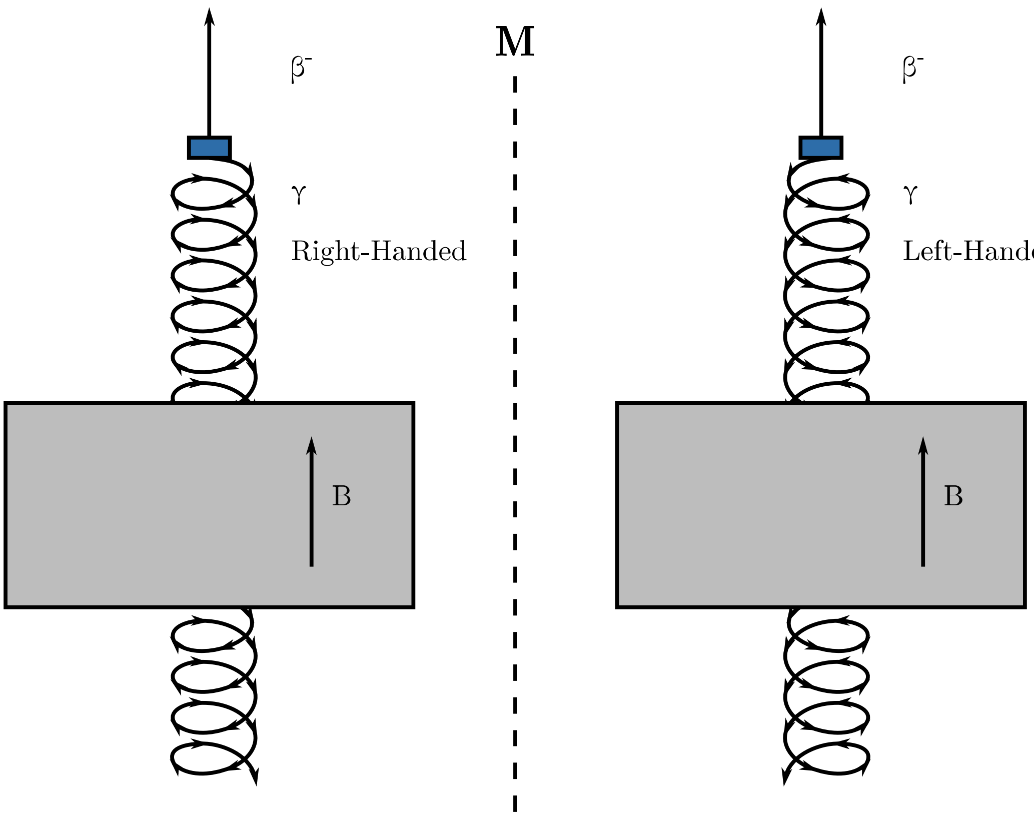

Figure 8. Circularly polarized gamma rays from ^{60}Co source and mirror image. After applying the mirror transformation, **M**, the beta particle and gamma ray emitted during the decay have the same momentum as before, but the direction of angular momentum of the gamma ray is switched, changing the right-handed gamma rays to left-handed.

In general, the distribution of gamma rays from a polarized ^{60}Co nucleus may be described by a distribution of the form described by Lipkin [22] of $1 + A\cos\theta$, where θ is the angle between the polarization axis of the nucleus and the momenta of the emitted gamma rays. Clearly, the two extremes of this are when $\theta = 0$ and $\theta = \pi$. The experiment described in this thesis corresponds to the case where $\theta = \pi$.

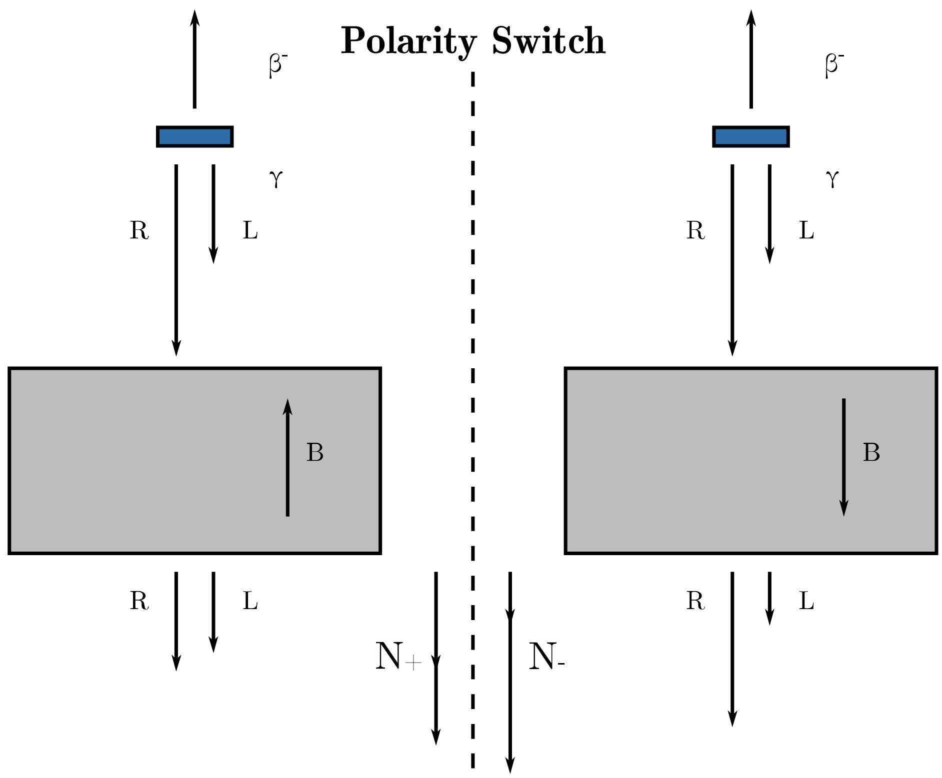

Figure 9. Filtering effect of the magnet on circularly polarized gamma rays. The lengths of the R and L arrows correspond to the relative count rates of right- and left-handed gamma rays emitted during ^{60}Co decay, for a specific gamma energy. Note that these are not drawn to scale according to the actual asymmetry of gamma rays produced in the decay. When the gamma rays pass through the magnet, they are attenuated by different amounts depending on the relative orientation of their angular momentum vectors and the magnetic field in the magnet. The counts N_+ and N_- represents the number of gamma rays that are transmitted through the magnet with a magnetic field in the positive or negative z-direction, respectively.

2.4. Asymmetry

The number of gamma rays transmitted through the attenuator for positive and negative polarities are defined as N_+ and N_-, respectively. Because the gamma rays emitted by ^{60}Co have two different energies, N_+ and N_- are different for each energy. In order to quantify the difference between the N_+ and N_-, the number of events for each energy for positive and negative magnet polarity, respectively, the quantity of asymmetry is defined as

$$E = \frac{N_+ - N_-}{\frac{1}{2}(N_+ + N_-)} . \tag{9}$$

The asymmetry can be used to show that parity is violated in ^{60}Co decay. If parity were not violated, N_+ and N_- would have equal values, and the asymmetry of the measurement would be 0. Thus, the asymmetry is a way to quantify the degree to which parity is violated in the decay.

2.4.1. Compton Cross-Section

When the gamma rays traverse the attenuator, there is a probability that they will scatter off of atomic electrons in the substance. The total Compton cross-section is given by

$$\sigma = \sigma_0 \pm fPZ\sigma_c\,, \tag{10}$$

where σ is the total Compton cross-section for scattering from electrons in a magnetically polarized substance, f is the fraction of oriented electrons in the material, P is the polarization of the gamma rays, Z is the number of electrons, σ_0 is the Klein-Nishna polarization-independent Compton cross-section for the material [23], and σ_c is the polarization-sensitive correction. The quantity fZ is the number of oriented electrons per atom, ν. The mass attenuation coefficient μ is given by

$$n\sigma_0 = \mu\rho\,, \tag{11}$$

where $n = \frac{N_a}{A}\rho$ is the electron density of the material, N_a is Avagadro's number, and A is the atomic mass of the material, and ρ is its mass density. The polarization-sensitive correction factor for the differential cross section is given by Schopper [13] and derived by Chesler [24] as

$$\sigma_c = 2\pi r_0 \left\{ \frac{1 + 4k_0 + 5k_0^2}{k_0(1 + 2k_0)^2} - \frac{1 + k_0}{2k_0^2} \ln(1 + 2k_0) \right\}, \qquad k_0 = \frac{E_\gamma}{m_e c^2}, \tag{12}$$

where $r_0 = 2.82\times10^{-13}$ cm is the Bohr radius, E_γ is the energy of the incident gamma ray, and $m_e c^2 = 511$ keV is the rest energy of an electron. For the gamma ray with energy $E_\gamma = 1.17$ Mev, $\sigma_c = -1.457\times10^{-26}$ cm^2, and for energy $E_\gamma = 1.33$ MeV, $\sigma_c = -1.682$ cm^2.

2.4.2. Transmission Through Attenuator

In order to compute the number gamma rays which are transmitted through the attenuator, it is assumed that the number of gamma rays produced by the decay is a mixture of left- and right-handed gamma rays, N_L and N_R, respectively. The total number of incident gamma rays, N_0, is given by

$$N_0 = N_L + N_R \,. \tag{13}$$

The linear attenuation through the rod is given by

$$\lambda_{\pm} = \mu\rho \pm nfPZ\sigma_c \,, \tag{14}$$

where $\lambda_{\pm}$ is the linear attenuation coefficient through the attenuator which depends on the relative orientation of the gamma ray angular momentum and the spin direction of the electrons in the attenuator. The coefficient λ_{+} corresponds to the scenario where the magnetic field is in the positive z-direction, which means that the spin of the electrons is oriented in the negative z-direction; the angular momentum of a right-handed gamma ray is also directed in the negative z-direction, meaning that λ_{+} corresponds to when the angular momentum of the gamma ray and the spin direction of the electron are parallel. The number of gamma rays transmitted through the attenuator is then given by

$$N_{\pm} = N_R e^{-\lambda_{\pm} x} + N_L e^{-\lambda_{\mp} x} = e^{-\mu\rho x}\left(N_R e^{\pm nfPZ\sigma_c} + N_L e^{\mp nfPZ\sigma_c}\right) , \tag{15}$$

where x is the thickness of the attenuating material. The gamma ray count N_{+} is the number of gamma rays transmitted through the iron rod when the magnetic field is directed in the positive direction (toward the source) and N_{-} is the number of gamma rays transmitted when the magnetic field was directed in the negative direction.

Substituting N_{+} and N_{-} into Eq. (9) yields the relation

$$E = \frac{(N_R - N_L)(e^{nfPZ\sigma_c x} - e^{-nfPZ\sigma_c x})}{\frac{1}{2}(N_R + N_L)(e^{nfPZ\sigma_c x} + e^{-nfPA\sigma_c x})} = 2\frac{N_R - N_L}{N_R + N_L}\tanh(nfPZ\sigma_c x) \,. \tag{16}$$

The fraction $P_0 = \frac{N_R - N_L}{N_R + N_L}$ was measured by Lundby, et al. [11] to be about 0.6 for ^{60}Co; thus, the expected asymmetry is given by

$$E = 2P_0 \tanh(nfPZ\sigma_c x)\ , \tag{17}$$

After substituting in $\nu = fZ$ and $n = \frac{N_a}{A}\rho$, the expected asymmetry may be written

$$E = 2P_0 \tanh\left(\frac{N_a \rho P \nu \sigma_c x}{A}\right). \tag{18}$$

2.5. Uncertainty

2.5.1. Uncertainty of Asymmetry

The uncertainty of the asymmetry with respect to the numbers of gamma rays parallel and antiparallel may be written

$$(\delta E)^2 = \left(\frac{\partial E}{\partial N_+}\delta N_+\right)^2 + \left(\frac{\partial E}{\partial N_-}\delta N_-\right)^2. \tag{19}$$

However, because this is a counting experiment, $\delta N_\pm = \sqrt{N_\pm}$; substituting this in and taking the partial derivatives yields the uncertainty in terms of N_+ and N_- as

$$\delta E = 4\frac{\sqrt{(N_-\delta N_+)^2 + (N_+\delta N_-)^2}}{(N_+ + N_-)^2} \tag{20}$$

$$\delta E = 4\sqrt{\frac{N_+N_-}{(N_+ + N_-)^3}}. \tag{21}$$

Note that this form assumes that the measurements of N_+ and N_- were taken for an equal amount of time.

To obtain a certain target uncertainty on the measurement, it must be assumed that $N_\pm$ has the form

$$N_\pm = R_\pm T\ , \tag{22}$$

where T is the collection time and $R_\pm$ is the count rate corresponding to parallel and antiparallel. Substituting this into the uncertainty and solving for T yields the expression

$$T = \frac{16R_+R_-}{(\delta E)^2(R_+ + R_-)^3}\,. \tag{23}$$

This may be simplified by introducing the average count rate $\bar{R} = \frac{R_+ + R_-}{2}$. It may be observed that $R_\pm = \frac{1}{2}(2 \pm E)\bar{R}$. Substituting $R_+ + R_- = 2\bar{R}$ into the denominator and $R_\pm$ into the numerator, it may be shown that

$$T = \frac{4(2+E)(2-E)\bar{R}^2}{(\delta E)^2\bar{R}^3} = \frac{4 - E^2}{(\delta E)^2\bar{R}}\,. \tag{24}$$

However, $\bar{R}$ may also be expressed as $\bar{R} = \frac{N_+ + N_-}{2T}$. Substituting in N_+ and N_- into this yields

$$\bar{R} = \frac{e^{-\frac{\mu}{\rho}x}}{2T}(N_R + N_L)(e^{nfPZ\sigma_c x} + e^{-nfPZ\sigma_c x})\,, \tag{25}$$

$$\bar{R} = \frac{e^{-\frac{\mu}{\rho}x}}{T}(N_R + N_L)\cosh(nfPZ\sigma_c x). \tag{26}$$

The count rate for the same geometry but no attenuating material, R_0, may be expressed as $R_0 = \frac{N_R + N_L}{T}$. Substituting this in yields

$$\bar{R} = R_0 e^{-\mu\rho x}\cosh(nfPZ\sigma_c)\,. \tag{27}$$

Substituting $\bar{R}$ into Eq. (24) yields

$$T = \frac{\frac{4}{E^2} - 1}{\left(\frac{\delta E}{E}\right)^2 R_0} \cdot \frac{e^{\mu\rho x}}{\cosh(nP\nu\sigma_c x)}\,, \tag{28}$$

where $\frac{\delta E}{E}$ is the target relative uncertainty. Furthermore, the expected asymmetry $E = 2P_0\tanh(nP\nu\sigma_c x)$. This yields the expected collection time as a function of the attenuator length x and the target uncertainty $\frac{\delta E}{E}$ as

$$T = \frac{\frac{1}{P_0^2\tanh^2(nP\nu\sigma_c x)} - 1}{\left(\frac{\delta E}{E}\right)^2 R_0} \cdot \frac{e^{\mu\rho x}}{\cosh(nP\nu\sigma_c x)}\,. \tag{29}$$

Multiplying through by $\left(\frac{\delta E}{E}\right)^2 R_0$ gives the collection time in units of decay events,

$$TR_0\left(\frac{\delta E}{E}\right)^2 = \frac{\frac{1}{P_0^2\tanh^2(nPv\sigma_c x)} - 1}{\cosh(nPv\sigma_c x)}\, e^{\mu\rho x}. \tag{30}$$

This is plotted in Figure 10, where $n = \frac{N_a}{A}\rho$. The values used to plot the function are given in Table 1.

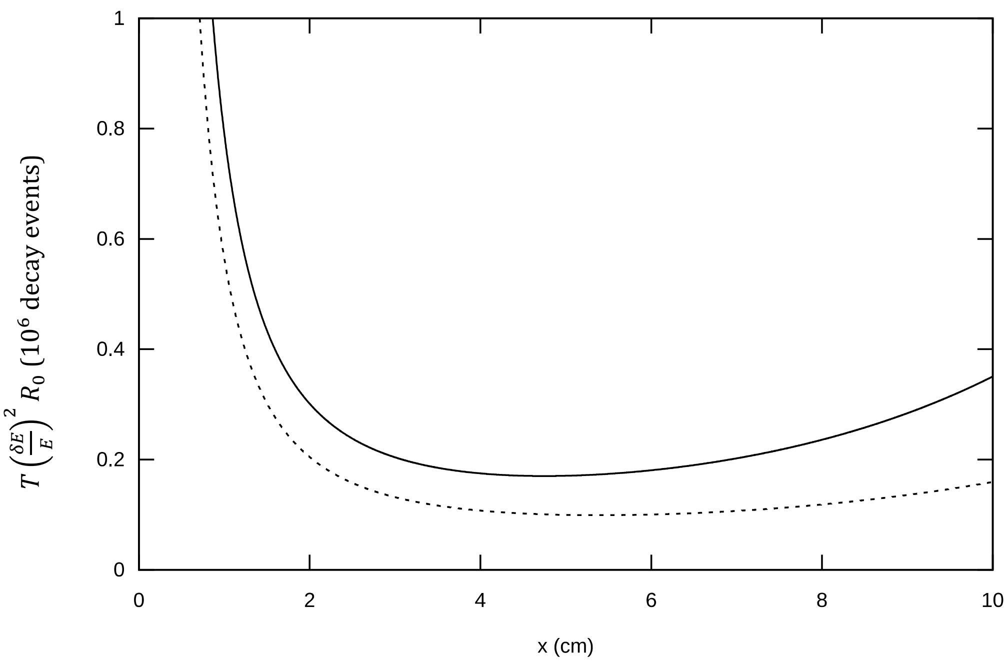

Figure 10. Graph of collection time as a function of attenuator length. The collection time is plotted in units of 10^6 decay events. The solid line is the time for the 1.17 MeV gamma ray, and the dashed line is for the 1.33 MeV gamma ray. It may be observed that the collection time is minimized for an attenuator length of about 5 cm.

From the collection times plotted in Figure 10, it is clear that there is a certain x for which the collection time is minimized for all relative uncertainties $\frac{\delta E}{E}$ at about 5 cm. This is approximately true for both energies. An exact value for both energies may be found by minimizing T analytically; however, because optimal values will differ between the two energies, in practice the best length of the attenuator will lie between the two optimal distances.

Table 1. Values of variables used to plot Eq. (31).

Variable	Value
A	$55.845\ \mathrm{g \cdot mol^{-1}}$
ρ	$7.15\ \mathrm{g \cdot cm^{-3}}$
P	1
ν	2.06
σ_c (1.17 MeV gamma ray)	$-1.457\times10^{-26}\ \mathrm{cm^2}$
σ_c (1.33 MeV gamma ray)	$-1.682\times10^{-26}\ \mathrm{cm^2}$
μ (1.17 MeV gamma ray)	$5.893\times10^{-2}\ \mathrm{cm^2 \cdot g^{-1}}$
μ (1.33 MeV gamma ray)	$5.196\times10^{-2}\ \mathrm{cm^2 \cdot g^{-1}}$

2.5.2. Temporal Variation

The experiment described in this thesis is designed such that the measurements of N_+ and N_- are taken at different times. This reduces differences in geometry that might arise if the two were measured at the same time but with a duplicate apparatus. However, the disadvantage of this approach is that variations in the background radiation levels may change over time. Furthermore, achieving low statistical uncertainties requires data collection for a long time, meaning even slow variations over time in background radiation or even electronic noise are significant.

Many long-term variations in background levels may be related to solar events. For example, variations in background levels may occur throughout the year as the sun experiences solar flares. Peterson, et al. [25] detected gamma radiation reaching earth with energy peaking around 200 to 500 keV from a solar flare. Additionally, solar flares occur in cycles, with a mean period of 154 days [26]. These cycles represent a problem because if the data collected for N_+ were taken between flares, but the data collected for N_- were taken during a flare, an asymmetry may be present between the two measurements that was not due to the asymmetry in the decay of the source but rather due to differences in background radiation during data collection.

An additional long-term variation, not related to background radiation, is possible drifting of the gain of electronic amplifiers. There are many different factors that may affect amplifier gain, such as temperature, meaning that it is difficult to predict or prevent changes in gain over time.

Another possible source of uncertainty may be fluctuations in the background light levels if there is a light leak. For example, if the data collected for N_+ was typically taken during the day, but the data collected for N_- were taken at night, it is possible that light leakage in the detectors would increase the number of accidentals in the N_+ dataset. In this scenario, even if no asymmetry was physically present, an asymmetry might be detected after performing data analysis. In other words, the additional accidentals counted in N_+ caused by light leakage might significantly affect the measurement of the asymmetry.

One way to reduce the effect of cyclic variations on the measurement is to use a data collection schedule which is mostly acyclic in duration. This does not reduce background levels, but does have the effect of equalizing the background levels between the measurements of N_+ and N_-; one method of doing so is discussed in Section 3.2.1.

Another method to reduce the effect of cyclic variations is to switch data collection between N_+ and N_- at a significantly faster rate than the rate at which variations occur. This technique approximates collecting data for N_+ and N_- "at the same time." Any variations in background levels would be evenly reflected in the count rates for N_+ and N_- using this technique. However, the drawback of this is that it increases the amount of dead time during data collection, as switching of the polarity of the magnet takes about one second; it was for this reason that acyclic schedule was chosen in this experiment instead of the fast switching schedule.

2.5.3. Ferromagnetic Hysteresis

In order to obtain the measurements N_+ and N_-, the magnetic field in the attenuator must be switched between two polarities. This is done by reversing the current in the electromagnet surrounding the iron rod. If the magnitudes of these currents are not equal, an asymmetry may be discovered between N_+ and N_- that can be attributed to the difference in the currents. Furthermore, because the polarity of the magnet is changed relatively frequently, as discussed in Section 3.2.1, it is important that the magnetic field does not deviate much from the ideal value.

However, this becomes more difficult to ensure with a ferromagnetic material such as iron. When an external field is applied to a ferromagnetic material, the magnetization of the material changes so as to partially align with the external field. Unlike a paramagnetic material, the magnetization of a ferromagnetic material is not directly proportional to the external magnetic field. This means that the relationship between the external magnetic field and the magnetization of the material exhibits hysteresis effects.

The relationship between the external magnetic field $\mathbf{H}$, the magnetization of the material $\mathbf{M}$, and the total magnetic field $\mathbf{B}$ is given by

$$\mathbf{H} = \frac{\mathbf{B}}{\mu_0} - \mathbf{M} \,.$$

In addition to $\mathbf{H}$ and $\mathbf{M}$ exhibiting hysteresis, $\mathbf{H}$ and $\mathbf{B}$ do as well [27]. This means that, for the same external magnetic field, $\mathbf{H}$, there are many different values which the total field $\mathbf{B}$ may have, depending on previous values of $\mathbf{H}$ and $\mathbf{B}$. An example of this may be seen in Figure 11, which shows a possible path of $\mathbf{B}$ in a ferromagnetic material as $\mathbf{H}$ is varied. As $\mathbf{H}$ increases, $\mathbf{B}$ follows a different path than as $\mathbf{H}$ decreases, demonstrating hysteresis.

This hysteresis effect is seen in an electromagnet with an iron core, which is used in the apparatus for this experiment. If $\hat{\mathbf{z}}$ is a unit vector along the axis of the cylindrical electromagnet poes, then $\mathbf{H}$ in the electromagnet is approximately given by

$$\mathbf{H} = \frac{nI}{l} \hat{\mathbf{z}} \,,$$

where n is the number of turns in the coil, l is the length of the coil, and I is the current through the wire in the coil. As the magnitude of $\mathbf{H}$ is proportional to I, it follows that $\mathbf{B}$ exhibits hysteresis as I is changed.

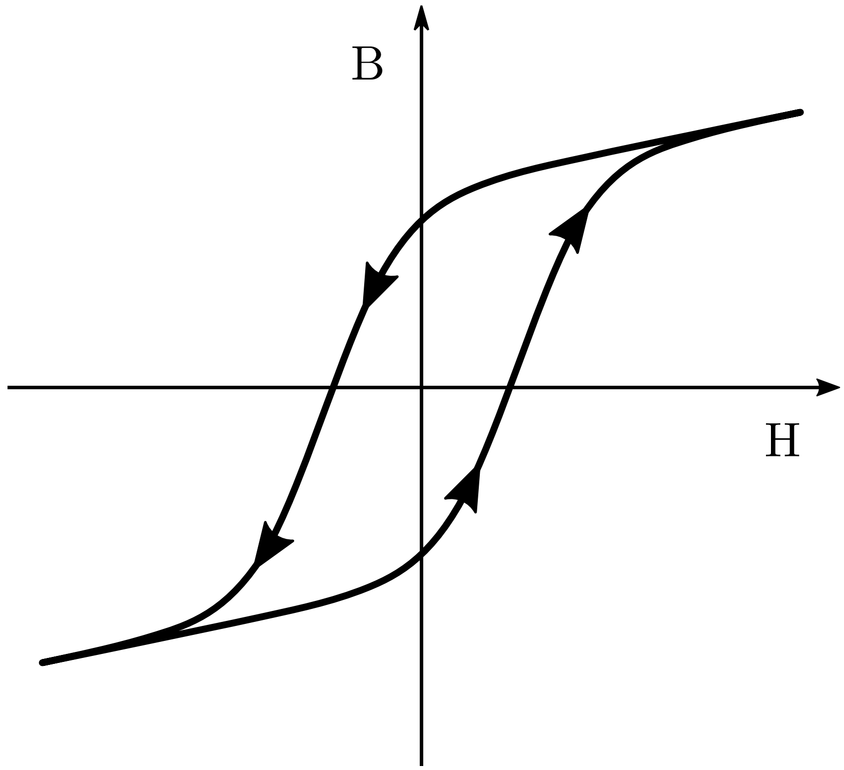

Figure 11. Graph illustrating the hysteresis of a ferromagnetic material. The arrows indicate the direction in which **H** and **B** are increasing or decreasing along each path. As a given material will have different properties, this is merely a representation of a possible path in $\mathbf{B} - \mathbf{H}$ space.

In practice, this means that it is difficult to precisely reverse the magnetic field in the iron rod used in the experiment described in this thesis. When the current in the electromagnet is cycled—reversing the direction of the current and then reversing it back to the original direction—the magnitude of the magnetic field will vary from the desired value, even if the magnitude of the current is the same. As the Compton scattering cross section depends on the magnetization of the iron rod, a variation in the magnetization while performing data collection results in a variation in the attenuation of the rod. Furthermore, the earth's magnetic field introduces a further asymmetry if not corrected for. In effect, the asymmetry and variation of the magnetic field translates to an uncertainty in the calculated asymmetry.

Chapter 3

EXPERIMENT AND APPARATUS

3.1. Setup

3.1.1. Introduction

In this chapter, the apparatus used to conduct the experiment is presented, and the experimental procedure is discussed. The apparatus and procedure are based on the experiment by Lundby, et al. [11]. A simple diagram of the apparatus may be seen in Figure 12.

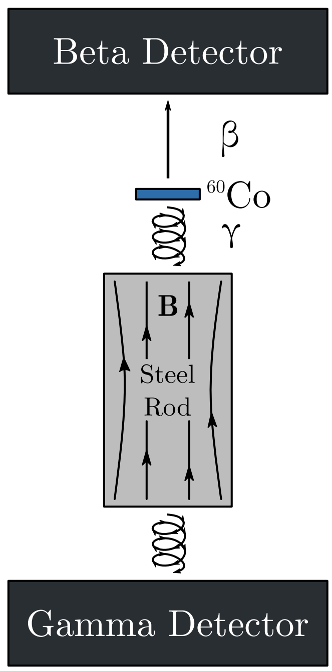

Figure 12. Simple diagram of apparatus. Beta particles that are emitted from the ^{60}Co source are detected by the beta detector, and gamma rays emitted in coincidence pass through the steel rod and are detected by the gamma detector.

The basic operation of the apparatus is to count the number of gamma rays emitted from the decay of ^{60}Co that pass through the iron rod, which is magnetized in either the positive or negative z-directions by the surrounding electromagnet, in coincidence with a beta particle emitted in the opposite direction. If a statistically significant asymmetry were measured between N_+ and N_-, the number of counts for the positive and negative directions of the magnetic field, respectively, it would indicate that there is an anisotropy in the distribution of gamma rays emitted from the decay of a polarized ^{60}Co source, implying that parity is violated in the weak interaction.

3.1.2. Physical Apparatus

The apparatus was designed to be cylindrically symmetric, with the detectors, source, and the iron rod placed collinearly along a single axis. An electromagnet was placed around the rod to magnetize it along the same axis in either direction, depending on the direction of current through the magnet.

A diagram of the apparatus used to conduct the experiment may be seen in Figure 13. When the ^{60}Co source decays, it emits a beta particle and two gamma rays, detected by the silicon and germanium detectors, respectively. The silicon detector (Ortec BA-014-025-1000) produces a pulse with nearly 100% efficiency when it is struck by a beta particle, but it is thin enough that the probability of detecting a gamma ray is about 0%. Due to the collinearity of the source, rod, and germanium detector (Tennelec ERVDS30-16215), the emitted gamma rays which pass through the steel rod are detected by the germanium detector, in addition to the gamma rays which scatter from other parts of the apparatus. The steel rod is magnetized in either the positive or negative z-directions; because the attenuation of the steel rod is slightly different for left- and right-handed circularly polarized gamma rays, it acts as a filter that may be used to determine the asymmetry between left- and right-handed gamma rays emitted from ^{60}Co decay. To reduce the number of accidental coincidences due to background radiation, lead shielding was placed around the germanium detector.

In order to ensure that the apparatus was as cylindrically symmetric as possible, acrylic mounts were used to rigidly hold the electromagnet, detectors, and source in place. These mounts were designed to be coaxial with the detectors, source, and steel rod. Masking tape was used to hold the steel plates on the top and bottom of the electromagnet.

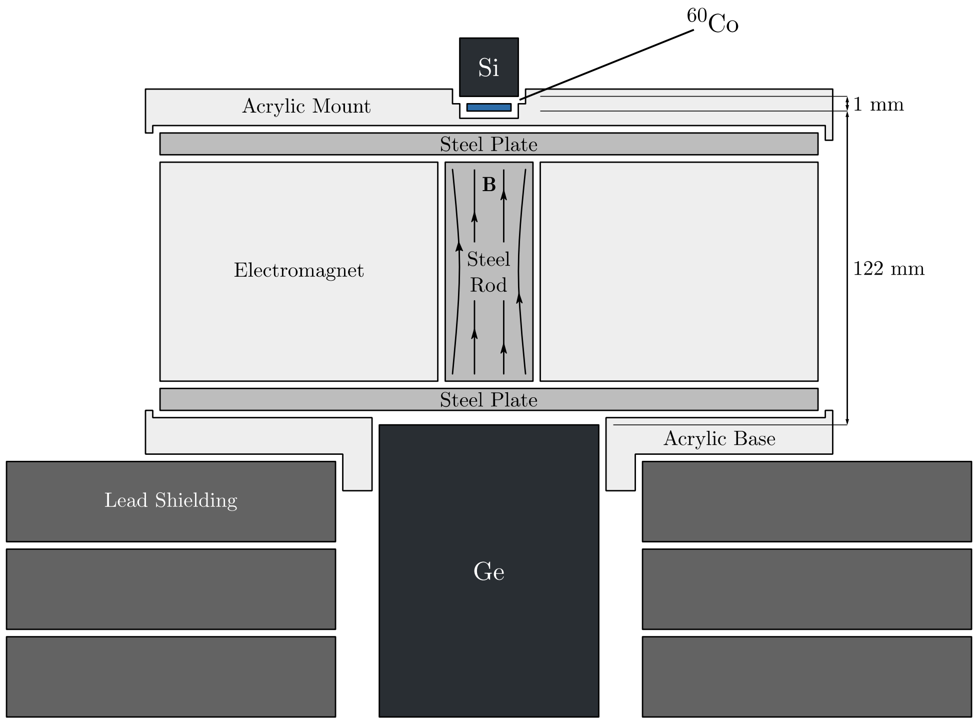

Figure 13. Cross section of the physical apparatus. ^{60}Co decay emits beta particles which are detected by the silicon detector. Coincident gamma rays are transmitted through the steel rod, magnetized by the electromagnet, and are detected by the germanium detector. The whole apparatus is ideally cylindrically symmetric.

3.1.3. Preparation of Source

The ^{60}Co was prepared by electroplating about 1 µCi of ^{60}Co in a $CoCl_2$ solution onto a stainless-steel foil. This foil was then glued using cyanoacrylic ("Krazy") glue between two thin polyethylene disks, each with a thickness of 0.8 mm and a diameter of 13 mm. Each disk had a central hole with a 5 mm diameter drilled out so that the source would be exposed when mounted between the disks.

3.1.4. Circuit

The counting circuit had both analog and digital components. The analog component, shown in Figure 14, consisted of the germanium and silicon detectors, preamplifiers for each, and Timing Filter amplifiers to bring the pulse heights into a range detectable by the digitizer and filter low frequency noise. The germanium detector (Tennelec ERVDS30-16215) was biased at −2900 V using a TC 950 high voltage power supply, and the silicon detector (Ametek BA-014-025-1000) was biased at +170 V using a Ortec 428 power supply. Pulses from the detectors were amplified by the preamplifiers; the germanium detector has a built-in preamplifier, and the silicon detector preamplifier was an Ortec 142. Timing filter amplifiers (Ortec 454) amplified the pulses to a range where their peaks were less than 1V; timing filter amplifiers were used instead of spectroscopy amplifiers in order to increase the timing resolution of the coincidence circuit.

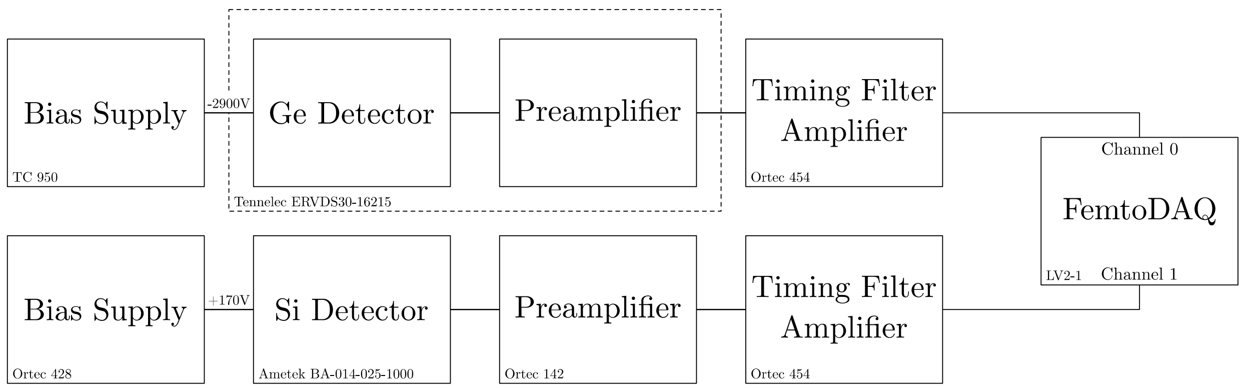

Figure 14. Block diagram of the NIM circuit. Note that the preamplifier for the Germanium detector is built into the device.

A fully analog coincidence circuit may be seen in Figure 15. While a digital version of the circuit was ultimately used to collect the data in this experiment, the analog version of the circuit was used during initial testing. It is shown here because it helps explain the operation of the digital version. Pulses originating from the germanium detector were filtered by a Constant Fraction Discriminator (Ortec 473A) and used to trigger the start input of a Time-to-Amplitude-Converter, or TAC (Ortec 437). If a filtered beta pulse occurred within a window of time, it triggered the stop input of the TAC, which produced an analog pulse. This was used as a gate to select only gamma pulses that were in coincidence with a beta pulse. These gamma pulses were then input a Multichannel Analyzer (Amptek MCA8000A). This produced an uncalibrated energy spectrum of only the detected gamma rays which occurred in coincidence with a detected beta particle.

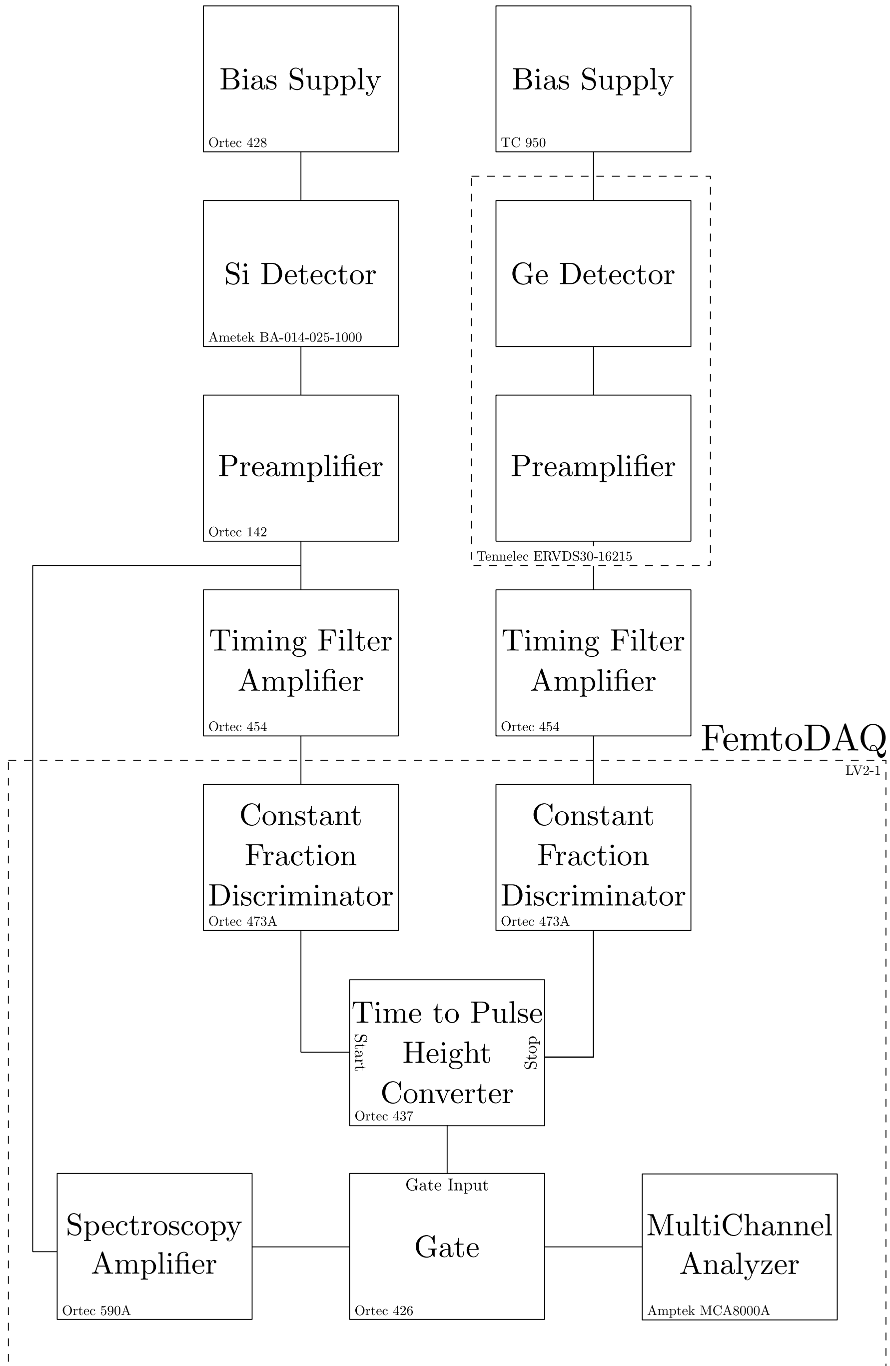

Figure 15. Block diagram of full coincidence circuit. The dashed box shows the portion of the circuit implemented digitally with a FemtoDAQ LV2-1 digitizer.

3.1.5. FemtoDAQ

The digital circuit was implemented using a FemtoDAQ LV2-1 multiparameter system. As shown in Figure 14, the amplified pulses from the germanium and silicon detectors were input directly into the two inputs of the FemtoDAQ. The device implements the coincidence portion of the circuit, as shown in Figure 15. Pulses from the germanium detector were used to trigger the device; when the device was triggered, it would record the time of collection and the heights of the pulses from the germanium and silicon detectors. After the collection period, these data could be "replayed" to produce a two-dimensional histogram of coincidence events.

The method by which the FemtoDAQ recorded events bears similarity to the analog coincidence circuit, with a few notable differences. The most significant difference is that the device does not trigger on pulses themselves, but on their derivatives. This has two consequences; first, low-voltage, high-frequency noise may trigger the device, resulting in higher background levels. Second, the derivative trigger results in a "soft" cutoff of on the energy histogram, due to a degree of non-uniformity between pulses. In other words, two pulses with the same maximum voltage may have slightly different derivatives, which may result in one pulse triggering the FemtoDAQ and the other pulse being ignored.

After a pulse has triggered the FemtoDAQ, digital representations of the voltage waveforms are analyzed to determine the pulse heights of the two inputs. Through a setting called "baseline restore," the software on the device ensures that the baseline of pulses is approximately 0, effectively removing low frequency noise from the input voltages. A setting known as the "pulse energy window" determines the range of time following the trigger to search for the maximum of each waveform; for this experiment, this was set to 1 μs. Finally, the input is averaged over a period of time in before the maximum value is determined according to a setting called the "signal averaging time," which for this experiment was set to 160 ns for the germanium detector and 10 ns (the time resolution of the device) for the silicon detector.

3.1.6. Electromagnet and Iron Rod

The electromagnet used to magnetize the iron rod was a Magnetech R-6030-24; the magnet had a diameter of 15.2 cm and a radius of 7.6 cm. The steel plate on top of the magnet had a thickness of 6.8 mm and the plate on the bottom had a thickness of 9.4 mm. The iron rod had a diameter of 2.5 cm, a height of 7.7 cm, and a density of $7.15\ \mathrm{g \cdot cm^{-3}}$. The density was measured by weighing on a scale and measuring the volume using a graduated cylinder filled with water, and was verified by measuring the dimensions of the cylinder and calculating the volume.

The electromagnet control circuit can be seen in Figure 16. The basic operation of the circuit was to supply current to the electromagnet from current-controlled source and to use a double-pole, double-throw (DPDT) relay (KHU 17D11-24V) to control the direction of the current. The relay was controlled using a voltage-controlled source. A single Hantek PPS2320A power supply was used to control both the DPDT relay as well as to power the magnet. The voltage and current outputs of the power supply were controlled by a computer through a USB connection. The current to the electromagnet was maintained at either ± 1.3 A (depending on the state of the DPDT relay) or 0 A, but the voltage varied depending on the temperature and resistance of the electromagnet. The typical voltage required to maintain this current was about 20 V, but as the coils in the electromagnet warmed up the voltage approached 30 V.

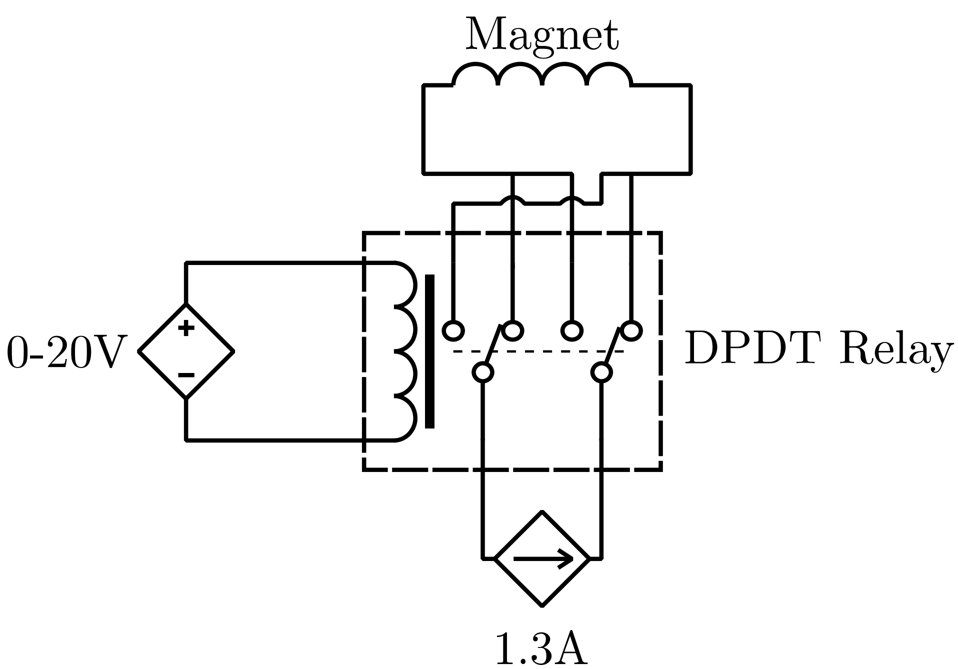

Figure 16. Control circuit for the electromagnet. The DPDT relay was used to switch the direction of current to the magnet.

3.2. Reduction of Systematic Uncertainty

3.2.1. Pseudo-Random Schedule

In order to avoid switching the magnet polarity in step with any of the potential cycles discussed in Section 0, a pseudo-random schedule was designed. This can be seen in Table 2. The number of hours was produced using the linear congruential generator

$$x_{i+1} = 8x_i + 5 \mod 7, \qquad x_0 = 0, \tag{31}$$

to generate the series $0, 5, 3, 1, 6, 4, 2, \ldots$, which has the property $x_i = x_{i+7}$. A second series was generated according to

$$y_i = x_i + 1, \tag{32}$$

which produced the series $1, 6, 4, 2, 7, 5, 3, \ldots$, with the property $y_i = y_{i+7}$. In order to ensure that both polarities received equal amounts of time, the series will be repeated twice and for each element of the series the polarity will be switched.

Table 2. Pseudo-random schedule. The schedule above was generated using a linear congruential generator. A complete cycle takes 56 hours, with each polarity being measured for 28 hours.

Hours	1	6	4	2	7	5	3	1	6	4	2	7	5	3
Polarity	+	-	+	-	+	-	+	-	+	-	+	-	+	-

3.2.2. Measurement of Magnetic Variation

As discussed in Section 2.5.3, the magnetization of the steel rod exhibits hysteresis because it is a ferromagnetic material. Figure 17 shows a measurement taken of this hysteresis. According to the schedule described in Section 3.2.1, the polarity of the magnet will be switched relatively frequently; however, the fact that the rod exhibits hysteresis means that it will be difficult to obtain exactly the same magnetization every time the magnet was switched. Thus, it was important that this variation be quantified and minimized; a histogram of the variation around the set points is shown in Figure 18.

To obtain the hysteresis cycle, the current was first set to zero, the relay was switched, and the current on the power supply was ramped to 1.3 A over about one second. The voltage across the relay was 20 V for positive polarity and 0 V for negative polarity. Throughout the process, the magnetic field was measured using a Vernier MG-BTA magnetic field sensor placed at a distance of about 8 cm from the top steel plate on the magnet, along the cylinder axis; the current was measured using a Vernier HCS-BTA High Current Sensor. Note that though the field was measured external to the iron rod, the field inside the iron rod should be proportional to the field external to it.

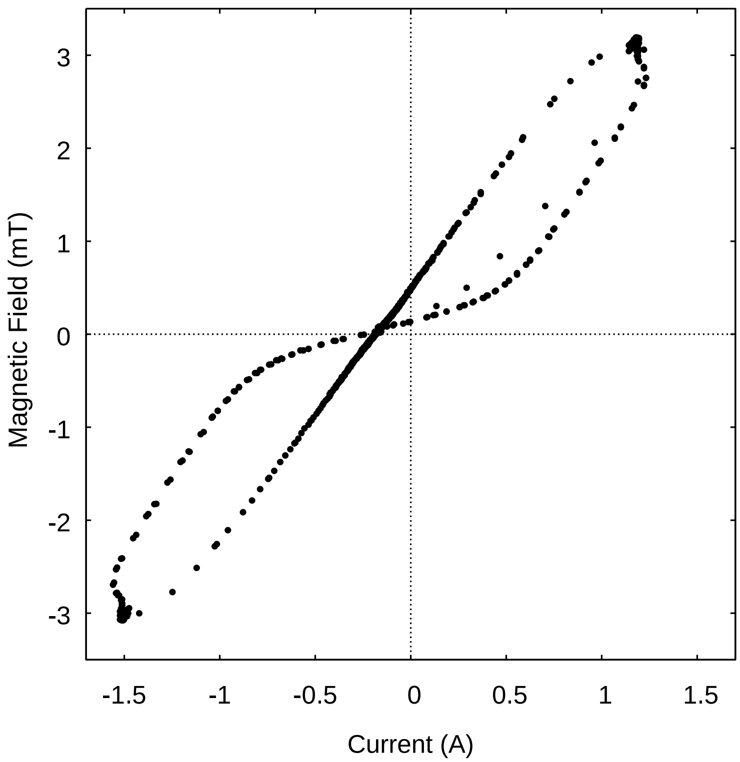

Figure 17. Graph of magnetic field in rod with changing current. The magnetic field was measured using a probe placed 8 cm from the top of the magnet. The lower path is due to increasing current, while the upper path is due to decreasing current.

The mean and standard deviation of the endpoints of the measured magnetic field shown in Figure 18 were computed to be -3.068 ± 0.0084 mT for negative polarity, and 3.181 ± 0.0044 mT for positive polarity. However, the earth's magnetic field at the experimental location (42.427374° N, 78.157070° W) is about -0.0495 ± 0.00017 mT [28]. Subtracting this from the measured fields yields -3.118 ± 0.0084 mT for the negative polarity and 3.132 ± 0.0044 mT for the positive polarity. The asymmetry of these values is given by

$$E_B = \frac{|B_+| - |B_-|}{\frac{1}{2}|B_+| + |B_-|}, \qquad \delta E_B = \frac{\sqrt{(\delta B_-|B_+|)^2 + (\delta B_+|B_-|)^2}}{(|B_+| + |B_-|)^2} \tag{33}$$

where $|B_\pm|$ is the magnitude of the magnetic field for positive and negative polarity and $\delta B_\pm$ is the associated uncertainty. These values are tabulated in Table 3 along the asymmetry of the magnetic field.

Table 3. Measurements of magnetic field and associated asymmetry. The magnetic fields measurements for the positive and negative polarities account for the effect of the earth's magnetic field.

Variable	Value
B_+	3.132 ± 0.0044 mT
B_-	-3.118 ± 0.0084 mT
E_B	0.0045 ± 0.00076

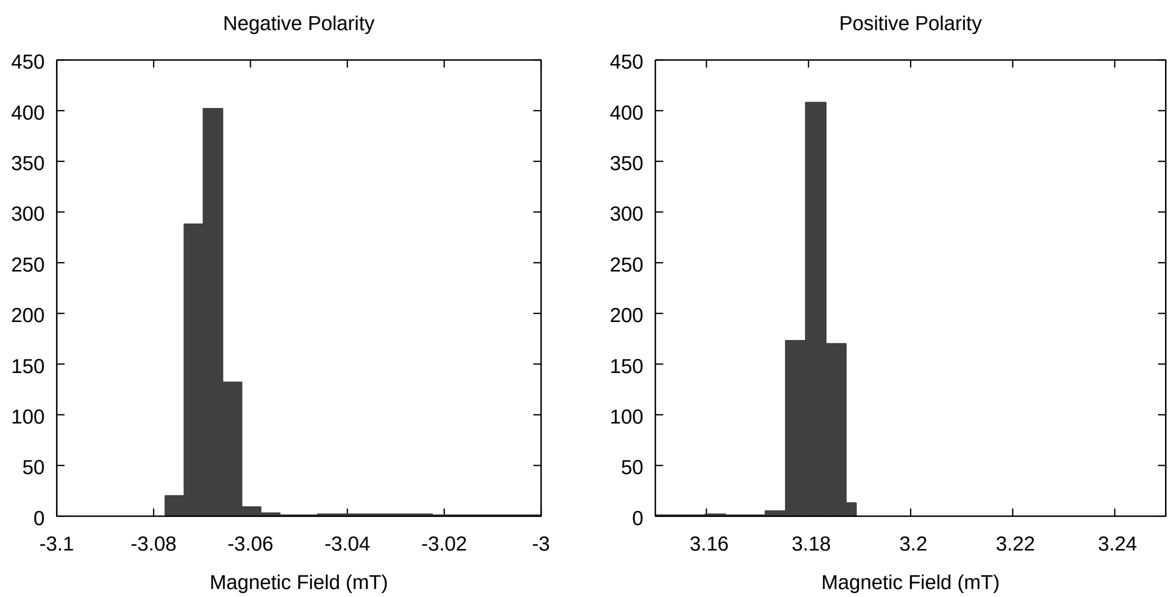

Figure 18. Measurements of the magnetic field for positive and negative polarities. Each measurement was performed by first cycling the current in the electromagnet and then setting it to ± 1.3 A. The mean and standard deviation was calculated to be -3.068 ± 0.0084 mT for negative current and 3.181 ± 0.0044 mT for positive current.

Depending on the desired statistical uncertainty of the asymmetry measurement, it may be necessary to compensate for the strength of the earth's magnetic field by adjusting the current through the electromagnet. However, as the iron rod in the electromagnet reaches saturation, the effect which the earth's magnetic field has on the magnetization decreases. In this experiment, it was assumed to be negligible and that any uncertainty it introduced would be significantly less than the statistical uncertainty of the experiment.

Chapter 4

RESULTS

4.1. Introduction

This chapter presents the results of a preliminary experiment using the apparatus described in the previous chapter. The asymmetry measured was found to disagree with the expected asymmetry, and the possibility of systematic error was explored. Finally, a survey of other sources of uncertainty is given, exploring the relative importance of each in the final measurement.

First, two coincidence histograms are shown for both polarities of the magnet, as well as the corresponding gamma singles spectra. The beta coincidence spectra are also shown. A lower threshold in the beta spectra is then defined, giving a coincidence gamma spectrum for each polarity. The 1.17 MeV and 1.33 MeV peaks in each of these spectra is then fit to a normalized Gaussian function with a linear background, giving the number of events in each peak. These are then used to determine the asymmetry of the measurement, and the corresponding uncertainty.

4.2. Data Collection and Calibration

Using the apparatus and procedures described in Section 3.1, preliminary experiments were carried out in order to demonstrate the effectiveness of the current experimental design. As described in Sections 3.1.4 and 3.1.5, the height of pulses from the germanium and silicon detectors were recorded every time a pulse from the germanium detector triggered the FemtoDAQ. These pulse heights were then plotted on a two-dimensional histogram.

The energy scales of the gamma energy spectra were calibrated using the 1.17 MeV and 1.33 MeV peaks of ^{60}Co decay; the beta energy spectra were not calibrated because there are no distinct energy peaks. Both polarities were collected over a 24 hour period, with a 26 hour period of no data collection between. During that time, the bin numbers of the two gamma energy peaks drifted by about 8%. Because of this, the energy scale of each spectrum was calibrated independently and Eq. (34) was fit to the peaks.

4.3. Energy Spectra

A two-dimensional energy spectrum of coincidences for both the positive and negative polarities of the magnet may be seen in Figure 19 and Figure 20, respectively. These spectra were each taken for 24 hours.

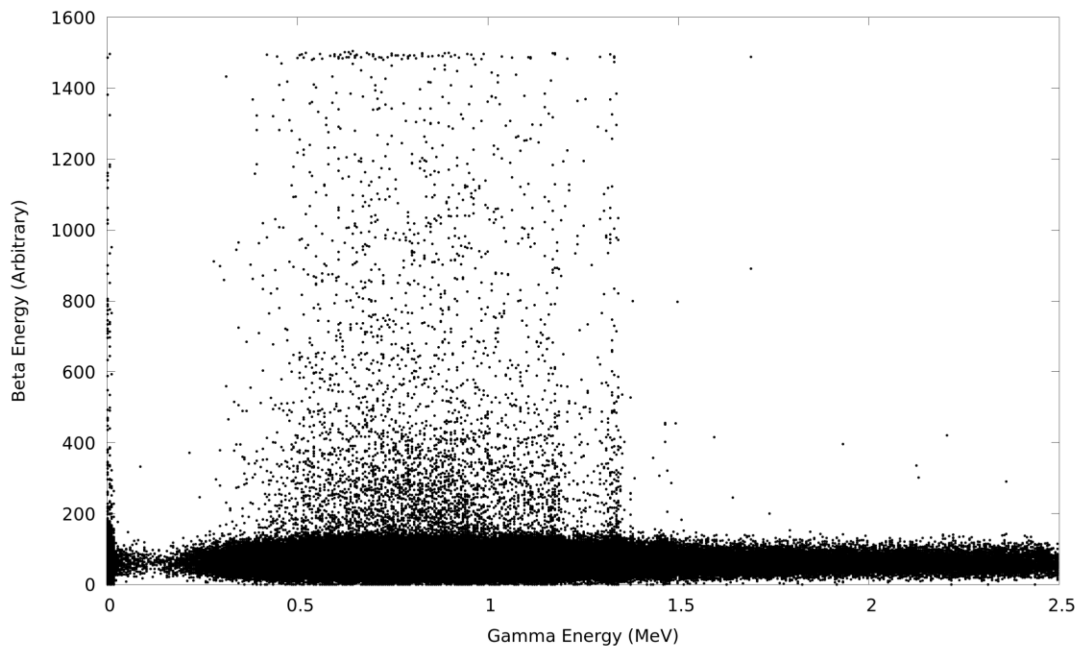

Figure 19. Histogram of gamma and beta energies, positive magnet polarity.
This spectrum was obtained over a 24-hour period.

A number of features may be observed in these spectra. First, a large horizontal band corresponding to low energy beta particles is present in each. The presence of this band is due to the triggering method; every time a pulse from the germanium detector triggered the FemtoDAQ, the pulse height of the silicon detector was recorded, regardless of the pulse height. Most of the time, the pulse from the silicon beta detector was not in coincidence with a pulse from the germanium gamma detector, and low-voltage electronic noise was recorded as the pulse height of the silicon detector. Another feature which may be observed in both spectra is a band corresponding to high energy beta particles, above which no events were observed. This band results from overflows, or pulses with maximum voltages higher than the maximum input voltage of the ADC on the FemtoDAQ, which was 1 V.

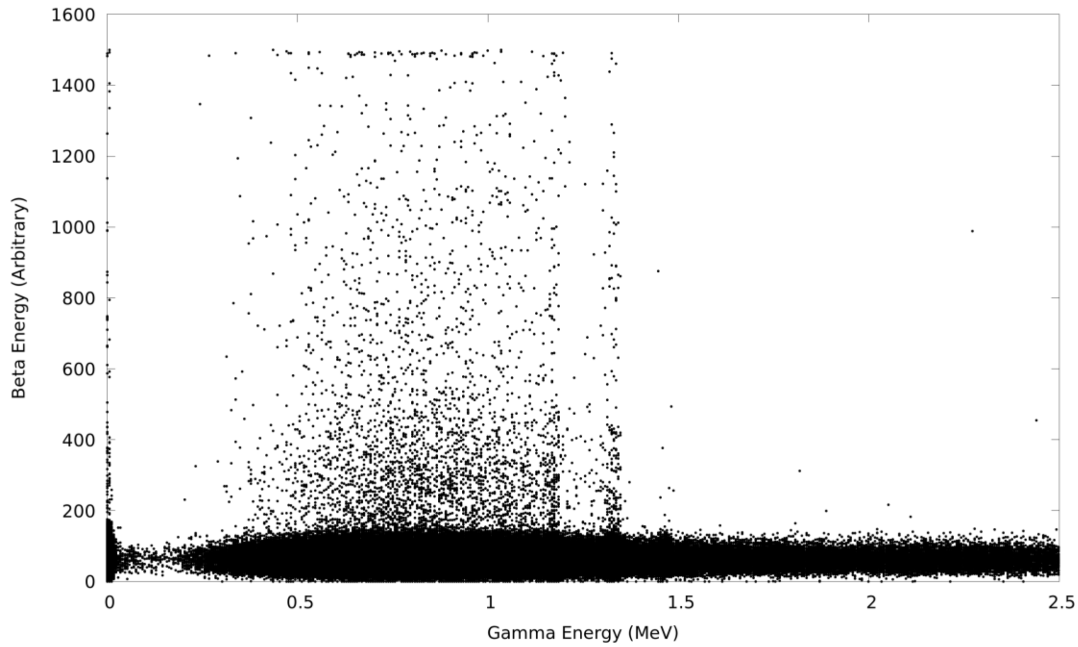

Figure 20. Histogram of gamma and beta energies, negative magnet polarity. This spectrum was obtained over a 24-hour period.

4.4. Data Analysis

In order to calibrate the gamma spectra, a normalized Gaussian function with a linear background

$$f(x) = mx + b + \frac{N}{\sqrt{2\pi\sigma^2}} e^{-\frac{(x-\mu)^2}{2\sigma^2}} \tag{34}$$

was fit to the singles gamma spectra, where x is the uncalibrated bin number on the spectrum, $mx + b$ is the linear background, N is the number of counts in the peak, σ is the standard deviation of the peak, and μ is the center channel of the peak. Fitting was performed using least squares by the Levenburg-Marquardt algorithm [29] with the program Gnuplot [30], and the uncertainty of each parameter was obtained from the covariance matrix of the fit.

Using the values of μ obtained for each peak, the gamma energy scale for each of the spectra was calibrated using a two-point calibration. This is given by

$$E(x) = \frac{E_1 - E_2}{\mu_1 - \mu_2}(x - \mu_1) + E_1 \,, \tag{35}$$

where x is the bin number, E is the calibrated energy corresponding to that bin, μ_1 and μ_2 are the centers of the peaks on the uncalibrated spectrum, and E_1 and E_2 are the energies corresponding to those peaks.

In addition to the obtaining a value for μ, the fit for each peak also gives an estimate for the number of events in that peak, N. In general, the number of events in a normalized Gaussian function is given by the integral

$$\int_{-\infty}^{\infty} \frac{1}{\sqrt{2\pi\sigma^2}} e^{\frac{(x-\mu)^2}{2\sigma^2}} dx = 1 \,. \tag{36}$$

Thus, in Eq. (34), N directly represents the number of counts in the peak, with the background removed. A typical fit to the 1.17 MeV peak in the gamma singles spectrum for a positive magnet polarity is shown in Figure 21. Note that the function was only fit to data between channel 210 and 230; for each fit, the channel range was chosen manually.

Table 4. Fits of $f(x)$ to the energy peaks in the singles gamma spectra of the 24 hour runs in Figure 19 and Figure 20. This is before applying the thresholds to the beta spectra.

Polarity	Energy	m (events $\cdot$ bin^{-1})	b (events)	N (events)	σ (bin)	μ (bin)
Positive	1.17 MeV	-73 ± 4.3	18100 ± 960	11800 ± 580	1.82 ± 0.087	219.44 ± 0.84
	1.33 MeV	-31 ± 4.6	9000 ± 1200	13300 ± 780	2.1 ± 0.12	249.1 ± 0.12
Negative	1.17 MeV	-91 ± 5.7	21000 ± 1200	15700 ± 740	1.67 ± 0.078	202.84 ± 0.077
	1.33 MeV	-41 ± 6.1	10000 ± 1400	1800 ± 1100	2.0 ± 0.12	230.2 ± 0.12

These values were used to calibrate the gamma energy scales of Figure 19 and Figure 20 according to Eq. (35). One important thing to note is that the bin number of the peaks shifted between the positive and negative polarities by about 20 channels. This is likely due to drifting of the gain of the amplifiers in the analog portion of the coincidence circuit.

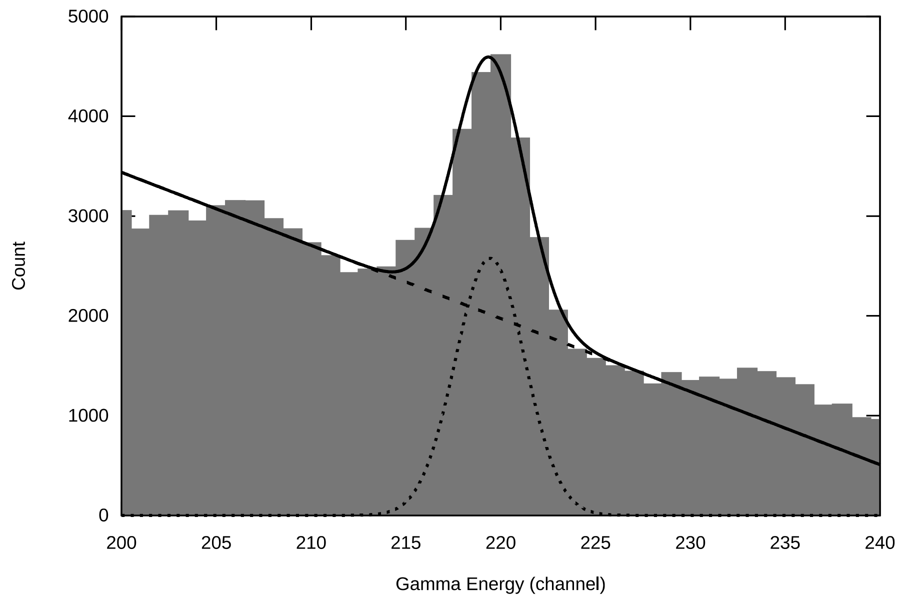

Figure 21. Typical fit used for calibration of gamma energy. Shown is the 1.17 MeV energy peak in the gamma singles spectrum for a positive negative polarity. The solid line is the full fit of a normalized Gaussian with a linear background, the dashed line is the linear background, and the dotted line is the normalized Gaussian.

The two gamma rays at 1.17 MeV and 1.33 MeV form bands in the two-dimensional spectra which correspond to peaks in the gamma spectra, shown in Figure 24 and Figure 25. The number of true coincidences in each band corresponds to N_+ and N_- for both magnet polarities. The counts N_+ and N_- were determined by the technique described in Section 0.

In Figure 22 and Figure 23, the projection of the coincidence spectra onto the beta energy axis may be seen. Below a bin number of about 150, the majority of pulses on the beta spectrum were due to electronic noise. To ensure that the events recorded were the result of a beta particle from the decay of ^{60}Co striking the silicon detector, and not the result of electronic noise, a threshold was defined at channel 150. This was then used to produce coincidence gamma spectra of all gamma rays which occurred in coincidence with a pulse from the silicon detector with a bin number greater than or equal to 150. These coincidence spectra may be seen in Figure 24 and Figure 25.

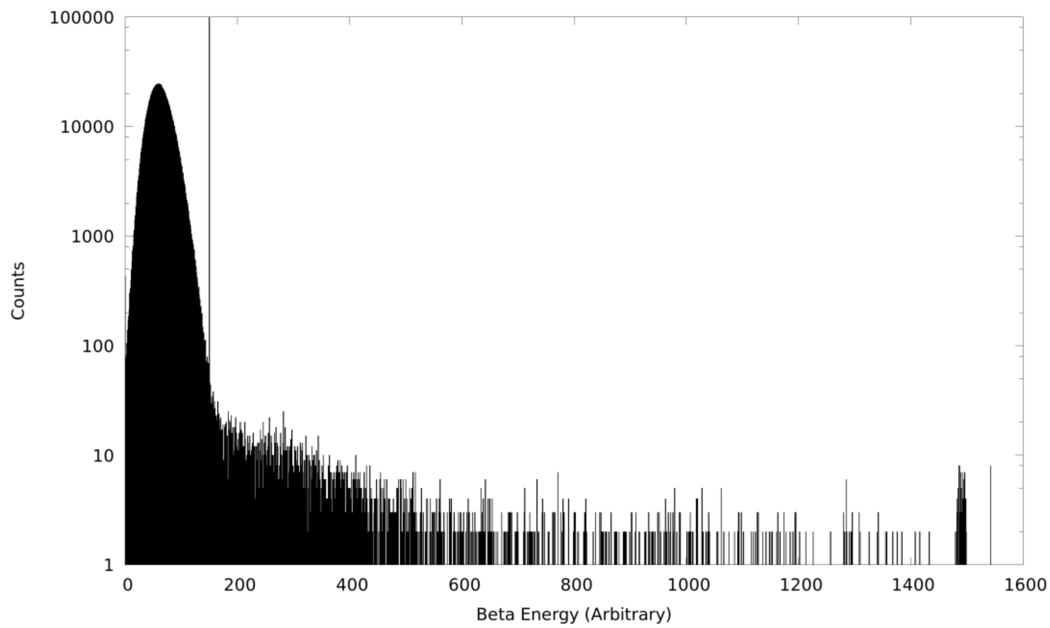

Figure 22. Projection of positive polarity coincidence histogram onto beta energy axis. The vertical line shows the threshold used to differentiate background radiation and electronic noise from pulses produced by beta particles.

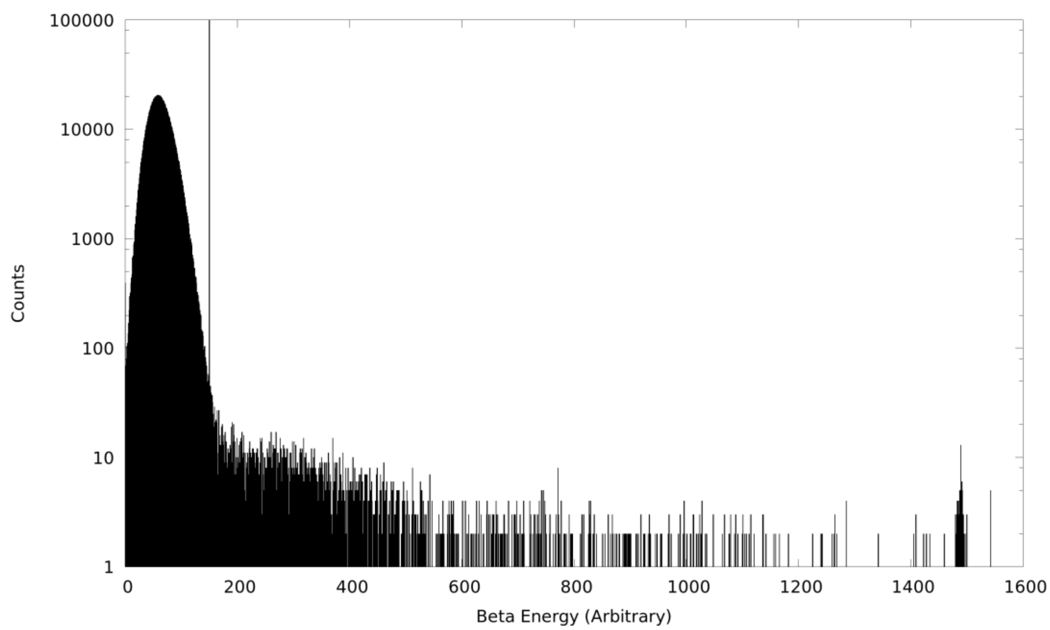

Figure 23. Projection of positive polarity coincidence histogram onto beta energy axis. The vertical line shows the threshold used to differentiate background radiation and electronic noise from pulses produced by beta particles.

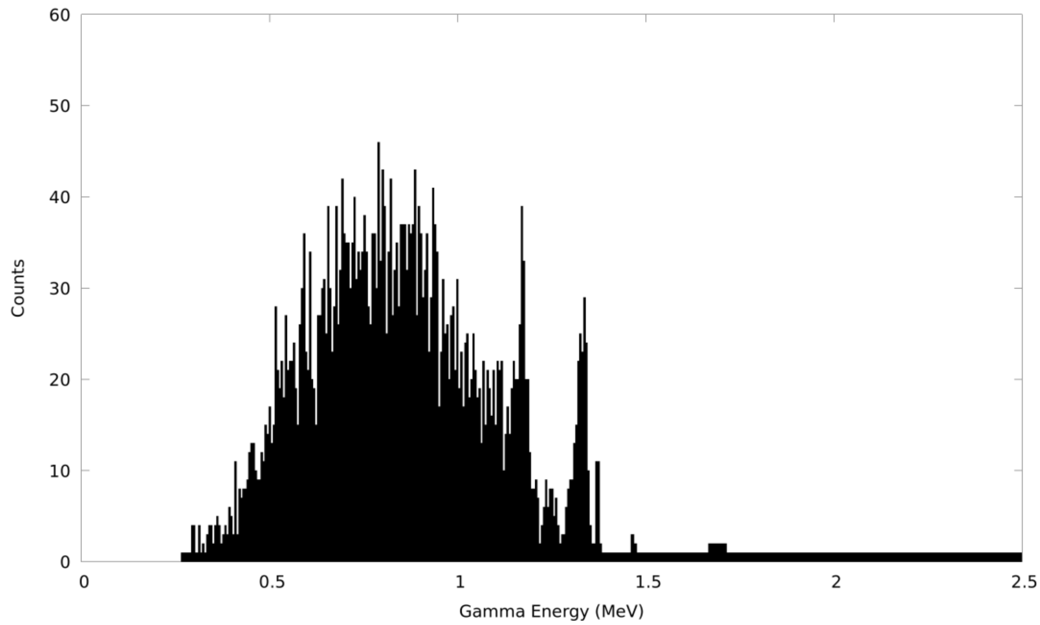

Figure 24. Projection of positive coincidence histogram onto gamma energy axis. These correspond to coincidence events with beta energy above the threshold described in the text.

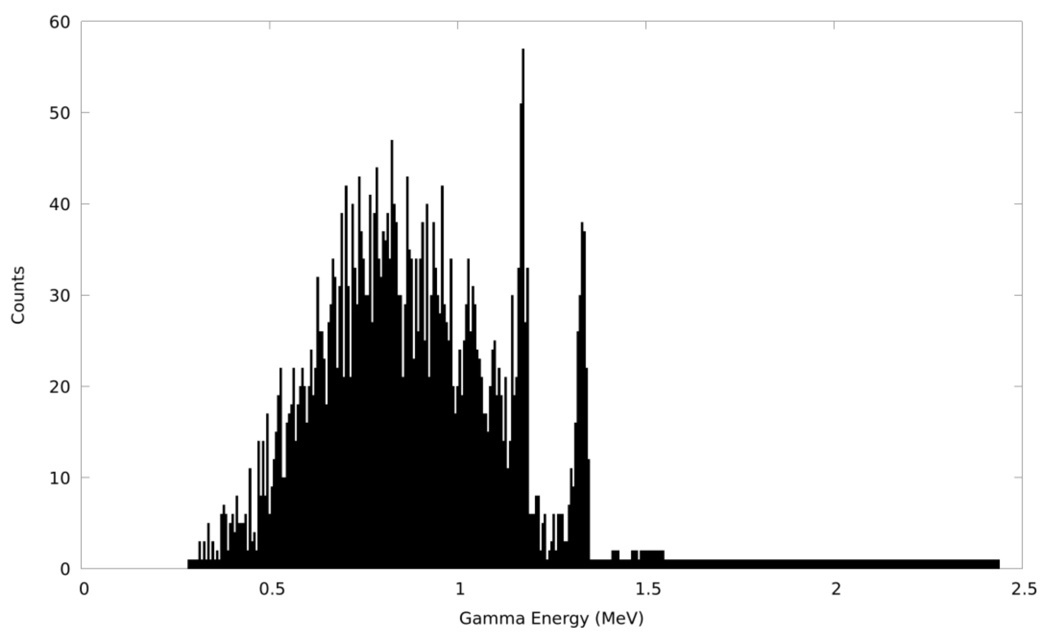

Figure 25. Projection of negative coincidence histogram onto gamma energy axis. These correspond to coincidence events with beta energy above the threshold described in the text.

4.5. Asymmetry

In order to determine the number of counts in each of the energy peaks of the gamma spectra after applying the threshold to the corresponding beta spectra, a normalized Gaussian with a linear background was fit to the peaks (on the uncalibrated gamma energy scale). The results may be seen in Table 5. A typical fit to the coincidence gamma spectrum may be seen in Figure 26.

Table 5. Fits of $f(x)$ to the energy peaks in the gamma spectra after applying the thresholds to the beta spectra. The spectra are shown in Figure 24 and Figure 25.

Polarity	Energy	m (events $\cdot$ bin^{-1})	b (events)	N (events)	σ (bin)	μ (bin)
Positive	1.17 MeV	-0.5 ± 0.13	120 ± 30	140 ± 25	2.7 ± 0.44	218.9 ± 0.40
	1.33 MeV	-0.2 ± 0.10	50 ± 26	140 ± 21	2.3 ± 0.30	248.5 ± 0.31
Negative	1.17 MeV	-0.7 ± 0.16	160 ± 34	150 ± 24	1.4 ± 0.23	202.5 ± 0.23
	1.33 MeV	-0.30 ± 0.087	70 ± 20	160 ± 17	1.7 ± 0.16	229.7 ± 0.19

The number of coincidences in each peak, N, in each peak may be seen in Table 6, along with the computed asymmetry for each energy peak. Although the Compton cross section is slightly different between each peak, the total of the two peaks is also shown. Although the relative uncertainty is large, for 1.17 MeV it is smaller than 100%, indicating that there is an asymmetry in the number of left- and right-handed gamma rays being emitted by ^{60}Co source.

Table 6. Coincidences in each energy peak of the coincidence gamma spectra, with associated asymmetry. The expected asymmetry was computed according to Eq. (18).

Energy	N_+	N_-	Asymmetry ($E \pm \delta E$)	Expected Asymmetry (E)
1.17 MeV	140 ± 25	150 ± 24	0 ± 0.2	-0.0261
1.33 MeV	140 ± 21	160 ± 17	-0.2 ± 0.18	-0.0301

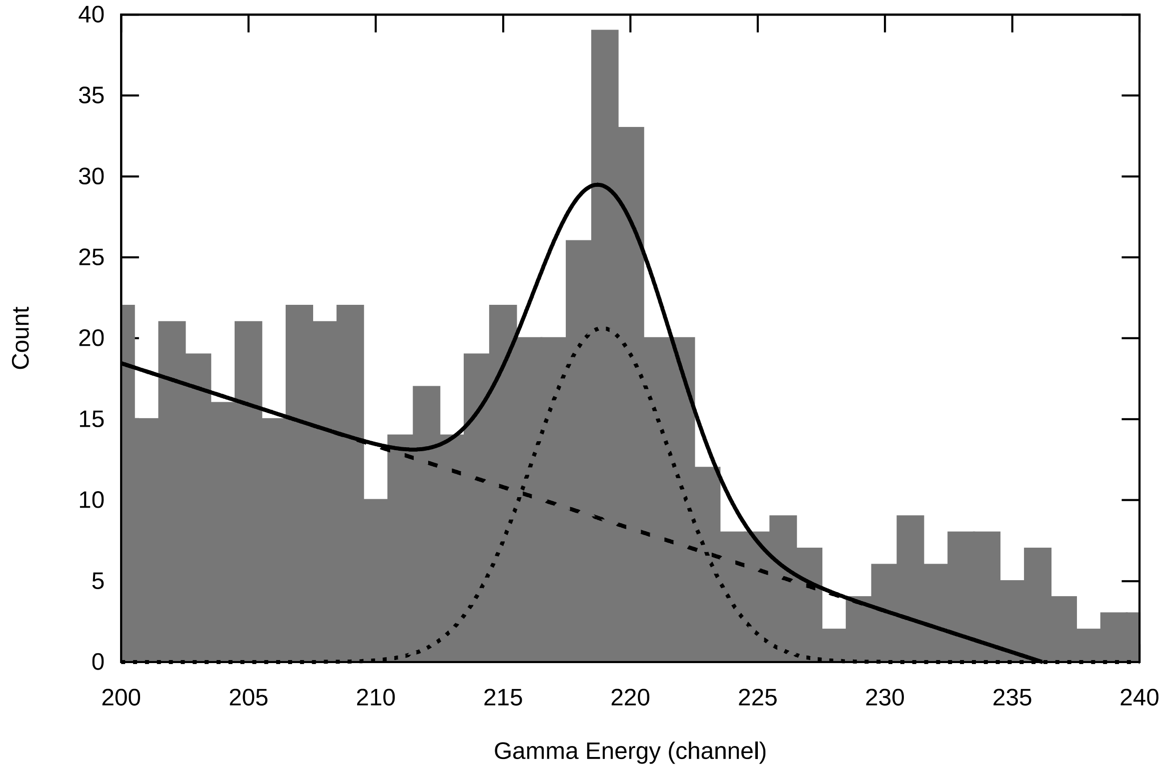

Figure 26. Typical fit of coincidence peak used to determine number of counts. Shown is the coincidence data for the 1.17 MeV gamma peak. The solid line is the combined normalized Gaussian fit with a linear background, the dashed line is the linear fit, and the dotted line is the normalized Gaussian.

In comparing the measured and expected asymmetries in Table 6, it is clear that these do not agree. For comparison, the number in each singles peak is shown in Table 7. As the singles spectra represent all gamma rays emitted from ^{60}Co, and not only those emitted in coincidence with a beta particle with vertical momentum, it is expected that there are equal numbers of left- and right-handed gamma rays in each peak. Thus, there should be no asymmetry; however, it was found that an asymmetry existed between the two spectra. Furthermore, in Table 8 the ratio $\frac{N_+}{N_-}$ is compared for each spectrum, showing some agreement between the singles and coincidence spectra.

It is possible that this asymmetry in both the singles and coincidence spectra may be due to a systematic error in data collection. The dead time remained below 1% for both of the runs, making it an unlikely source of error. However, the partial agreement between the ratios of $\frac{N_+}{N_-}$ for the coincidence and singles spectra indicate that a systematic source of error is likely.

Table 7. Coincidences in each energy peak of the singles gamma spectra, with associated asymmetry. The expected asymmetry was computed according to Eq. (18).

Energy	N_+	N_-	Asymmetry $(E \pm \delta E)$	Expected Asymmetry (E)
1.17 MeV	11800 ± 580	15700 ± 740	-0.28 ± 0.066	0
1.33 MeV	13300 ± 780	1800 ± 1100	-0.33 ± 0.082	0

Table 8. Ratios of $\frac{N_+}{N_-}$ for singles and coincidence spectra, with uncertainty given by $\frac{N_+}{N_-}\sqrt{\left(\frac{\delta N_+}{N_+}\right)^2 + \left(\frac{\delta N_-}{N_-}\right)^2}$.

Energy	$\frac{N_+}{N_-}$ (Singles)	$\frac{N_+}{N_-}$ (Coincidence)
1.17 MeV	0.75 ± 0.051	0.9 ± 0.22
1.33 MeV	0.72 ± 0.061	0.8 ± 0.15

4.6. Uncertainty Analysis

4.6.1. Count Rate Uncertainty

One of the most significant sources of error in the asymmetry is the statistical uncertainty due to the number of counts in each peak. First, because no background spectrum was collected, any attempt to count the number of events in each peak will also count background events. Furthermore, the drifting of the pulse heights between the gamma spectra means that different thresholds must be used on the uncalibrated spectra. Because the number of counts in each peak was determined by fitting the peaks to Gaussian distributions with linear backgrounds, the uncertainty in the number of counts is entirely due to the uncertainty of the fit parameters.

4.6.2. Uncertainty Due to Variations in Magnetic Field

As mentioned in Section 2.5.3, the asymmetry of the magnetic field produced by the electromagnet was computed to be 0.0045 ± 0.0008. This is about one tenth of the expected asymmetry; consequently, it only becomes important when the target statistical relative uncertainty is about 10%. This is significantly below the relative uncertainty of the results given in this thesis, and therefore is not significant for this experiment. However, the asymmetry of the magnetic field may represent a lower bound on the statistical uncertainty of future experiments.

One difficulty in measuring the asymmetry of the magnetic field was that it could only be measured externally at a distance of about 7 cm. While the field outside of the electromagnet is assumed to be proportional to the field in the iron rod, this is not necessarily the case. This means that the measurement of the asymmetry of the magnetic field outside the electromagnet is a rough estimate of the asymmetry of the magnetic field in the iron rod; if a low relative uncertainty is desired (less than 10%), it may be necessary to obtain a better estimate of the magnetic asymmetry using a probe closer to the iron rod.

Chapter 5

CONCLUSIONS

5.1. *Summary of Results*

In this thesis, an experiment to measure parity violation in ^{60}Co decay was described. The apparatus used to run the experiment was based on the one used by Lundby, et al. [11] and was designed to be used in undergraduate laboratories. The apparatus used a magnetized steel rod to measure the asymmetry of left- and right-circularly polarized gamma rays in coincidence with beta particles emitted from the decay of an unpolarized ^{60}Co nucleus. The asymmetry measured in preliminary experiments was found to have a large statistical uncertainty for both gamma ray energies. This uncertainty was largely due to a high uncertainty in the fit parameters. Furthermore, a statistically significant asymmetry between singles gamma rays was found that was not expected, indicating the presence of a systematic error.

Apart from statistical uncertainties, an attempt was made to minimize potential sources of systematic uncertainty. After measuring the asymmetry of magnetic hysteresis, it was found that the error it introduces is relatively small, meaning it may be insignificant for certain target uncertainties. Temporal variation of background radiation, on the other hand, was shown to be difficult to quantify, but two different techniques for minimizing the error it introduced were described, either by using a pseudo-random schedule for measuring N_+ and N_- or by switching between the measurements rapidly.

5.2. *Effectiveness of Apparatus*

There were two specific advantages to the apparatus used to conduct the experiment. First, the apparatus does not require a polarized target. A polarized ^{60}Co target requires cryogenic cooling of the radioactive source, which is relatively inaccessible to undergraduate laboratories, for whom this experiment was designed. Additionally, the use of a FemtoDAQ digitization device greatly simplifies the electronics, replacing most of the analog circuitry with a single device. Furthermore, the use of a FemtoDAQ allows the pulse heights of all events to be stored, increasing the flexibility of later data analysis.

5.3. Future Work

5.3.1. Introduction

This experiment was part of ongoing research in the design of a parity violation experiment for undergraduate laboratories. Consequently, there are a number of different aspects of the experiment that may be improved in the future. The most important will be minimization of uncertainty in the experiment. This will include investigation of methodology and longer data collection times. Other work will involve changing the geometry of the experiment, including the length of the steel rod and the germanium detector.

5.3.2. Minimization of Uncertainty

The most significant issue with this experiment was the uncertainty of the asymmetry measurement. As a background spectrum was not collected, the removal of background coincidences from the energy peaks in the gamma spectra was done using function fits of the peaks and the background. This introduced a significant amount of uncertainty into the estimation of the number of counts in each peak, ultimately increasing the uncertainty of the asymmetry measurement. Future work should refine the data collection process so that background spectra are collected.

An additional source of uncertainty is the drifting of the pulse heights of the peaks. While the drifting of the peaks in the gamma spectra was clear, it is difficult to quantify drifting of the beta spectra. This is significant because drifting of the beta energy may change the number of pulses above the threshold set for coincidence. If this were the case, the number of coincidences in each peak would show an asymmetry due only to the drift in the beta energy spectrum. In the future, an analysis of the drifting of the analog amplifiers should be performed, and amplifiers with minimal drift should be chosen to reduce the effect of drifting on the final result. Additionally, if possible the analog amplifiers should be removed from the digital coincidence circuit, as this would minimize the drifting of pulses heights.

5.3.3. Longer Data Collection Time

As discussed in Section 2.5.1, the relative uncertainty of the asymmetry is proportional to $1/\sqrt{T}$, where T is the collection time. This means that a reduction in the target relative uncertainty by a factor of two corresponds requires a collection time four times longer. Using this principle, it is estimated that a relative uncertainty of about 25% will take about 30 days. Future work will focus on running the experiment for longer in order to reduce this uncertainty.

5.3.4. Ideal Magnet Size

It was shown in Section 2.4.2 that the ideal length of the iron rod is about 5 cm. This length decreases the required collection time, for any desired statistical uncertainty of the measured asymmetry. In this experiment, the length of the iron rod was about 7.7 cm; subsequent experiments may use a shorter rod closer to the ideal length of 5 cm. Additionally, the difference in collection time between the two lengths should be estimated so as to estimate the advantage of shortening the rod.

5.3.5. Replacing the Germanium Detector with a Sodium Iodide Detector

Although the current apparatus utilizes a germanium detector to detect gamma rays from ^{60}Co decay, it does not fit the original goal of creating an experiment that uses equipment accessible to undergraduate laboratories. In addition to the high cost of the detector itself, the germanium detector requires cryogenic cooling, which is done using liquid nitrogen and a Dewar flask. Because of this, it is relatively expensive to obtain and operate, making it the most expensive part of the apparatus. The germanium detector may be eliminated by replacing it with a sodium iodide detector; however, this replacement would produce a significant reduction in energy resolution.

Appendix A

PHOTOGRAPH OF APPARATUS

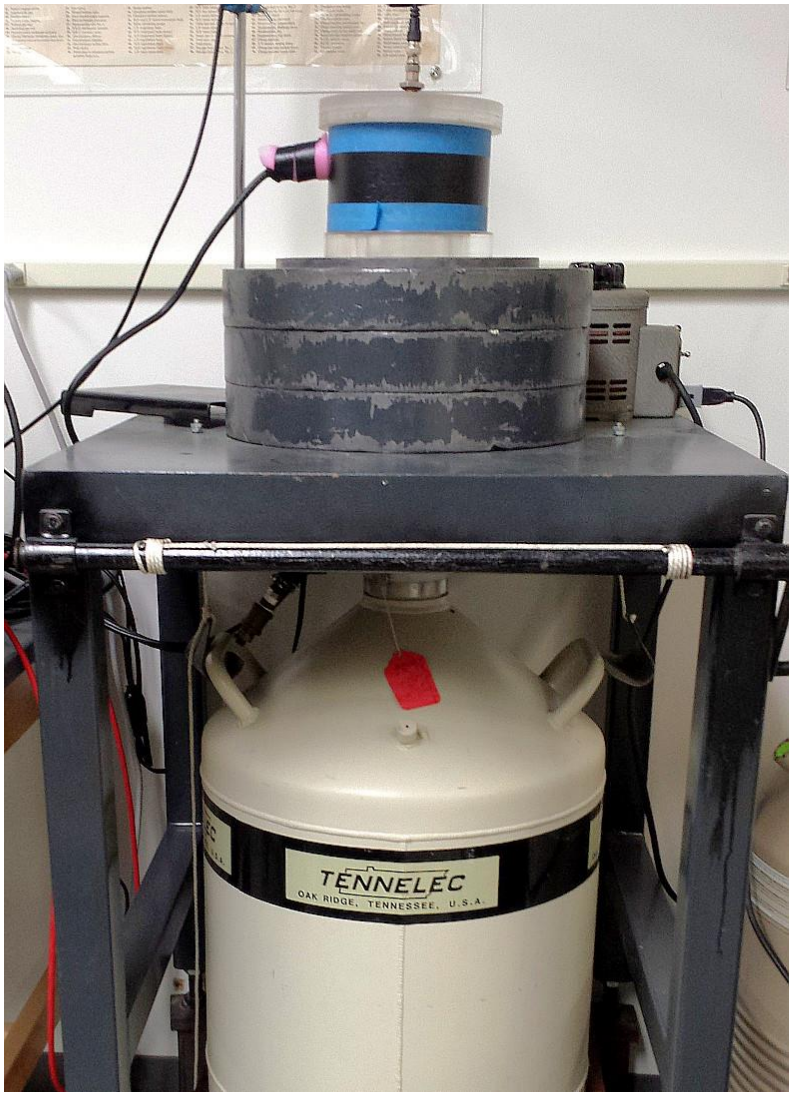

Figure 27. Photograph of the apparatus used to perform experiment.

Appendix B

DATA COLLECTION CODE

```
#!/usr/bin/python

# histogram_ex.py
# (c) 2016 SkuTek Instrumentation
# Author: D. Hunter
#
# versions:
#   0.1 01/26/16    - initial version based on get_histogram.py
#   0.2 04/07/16 DH - update for library changes
#
# Capture histogram data from the DDC-2 on inputs 0 and 1
# Create a gnuplot compatible text file with the data
#

import sys
from FemtoLib import *           # import the Digitizer class
from time import time,sleep
from digi_setup import *
import numpy as np
from power import SimplePowerSupply

# return the time in nanoseconds as an integer
def now():
    return int(1e9*time())

def take_energy_log(digi):
    t0 = now()
    t1 = t0 + 1000000000
    digi.StartCapture()
        while now() < t1:
                sleep(0.001)

    data       = digi.GetEnergyLog()
    time_stamp = digi.GetEnergyLogTimeStamp()*10
    dead_time  = digi.GetEnergyLogDeadTime()*10
    count      = digi.GetEnergyLogCount()

    return np.array(data, dtype='uint64'), t0, time_stamp, dead_time, len(data)


def write_data(data, time_stamp, *files):
    idx = np.argsort(data[:,0])
    data[:,0] = data[:,0]*10 + time_stamp

    for f in files:
        np.savetxt(f,data[idx],'%d')
        f.flush()

if __name__ == '__main__':
    try:
        settings_file, runtime, outfile = sys.argv[1:4]
        schedule = sys.argv[4] if len(sys.argv) >= 5 else None
        digi,conf = read_settings_file(settings_file)
```

```
            runtime  = int(runtime)
        except ValueError as e:
            print 'Usage: histogram.py <settings_file> <time_sec> <output_file> [<schedule>]'
            sys.exit()

        print_settings(digi)
        print "Writing to " + outfile

        fwStr = digi.GetFirmwareString()
        ADCtype = digi.IdentifyADC()

        print 'Digitizer firmware revision:', fwStr
        print 'Initializing ADC',ADCtype

        prep_digitizer(digi)
        sleep(0.1)

        # Set up the powersupply
        if schedule:
            supply = SimplePowerSupply('/dev/USB0')

        with open(outfile, 'wb') as f:
            total_time = 0
            dead_time = 0
            n = 0

            runtime = int(runtime * 1e9)
            end = now() + runtime

            while now() < end:
                data, time_stamp, t, dt, count = take_energy_log(digi)
                if count > 0:
                    write_data(data,time_stamp,f)
                    n          += count
                    total_time += t
                    dead_time  += dt
                    m1,m2 = data[:,1:].mean(axis=0)
                    print "{:20d} {:20d} {:4.2f} {:10.2f} {:10.2f}".format(time_stamp, n, floa
t(dead_time)/total_time, m1, m2)
                    sys.stdout.flush()

        digi.close()
```

R e f e r e n c e s

[1] E. Noether, Math. Ann. **77**, 89 (1915).
[2] O. Laporte and W. F. Meggers, J. Opt. Soc. Am. **11**, 459 (1925).
[3] C. N. Yang, Sci. **127**, 565 (1958).
[4] T.-D. Lee and C.-N. Yang, Phys. Rev. **104**, 254 (1956).
[5] J. Smith, E. Purcell, and N. Ramsey, Phys. Rev. **108**, 120 (1957).
[6] C.-S. Wu, E. Ambler, R. Hayward, D. Hoppes, and R. P. Hudson, Phys. Rev. **105**, 1413 (1957).
[7] T.-D. Lee, (1957), https://www.nobelprize.org/nobel_prizes/physics/laureates/1957/lee-speech.html.
[8] C. N. Yang, (1957), https://www.nobelprize.org/nobel_prizes/physics/laureates/1957/yang-speech.html.
[9] K. Myneni, (1984), http://ccreweb.org/documents/parity/parity.html.
[10] G. L. Trigg, *Landmark experiments in twentieth century physics* (Crane, Russak, and Company, Inc., 1975).
[11] A. Lundby, A. Patro, and J.-P. Stroot, Il Nuovo Cimento **6**, 745 (1957).
[12] M. Goldhaber, L. Grodzins, and A. Sunyar, Phys. Rev. **106**, 826 (1957).
[13] H. Schopper, Nucl. Instr. **3**, 158 (1958).
[14] R. L. Garwin, L. M. Lederman, and M. Weinrich, Phys. Rev. **105**, 1415 (1957).
[15] J. I. Friedman and V. Telegdi, Phys. Rev. **106**, 1290 (1957).
[16] H. Frauenfelder, R. Bobone, E. Von Goeler, N. Levine, H. Lewis, R. Peacock, A. Rossi, and G. De Pasquali, Phys. Rev. **106**, 386 (1957).
[17] J. Jackson, S. Treiman, and H. Wyld Jr, Phys. Rev. **106**, 517 (1957).
[18] H. Daniel and G. W. Eakins, Phys. Rev. **117**, 1565 (1960).
[19] R. M. Steffen, Phys. Rev. Lett. **3**, 277 (1959).
[20] M. Goldhaber, L. Grodzins, and A. Sunyar, Phys. Rev. **109**, 1015 (1958).
[21] H. M. Staudenmaier, *Physics Experiments Using PCs* (Springer-Verlag, 1993).
[22] H. J. Lipkin, *Beta decay for pedestrians* (North-Holland Publishing Company, 1962).
[23] O. Klein and T. Nishina, Z. Phys. **52**, 853 (1929).
[24] R. Chesler, Nucl. Instr. Meth. **37**, 185 (1965).
[25] L. E. Peterson and J. Winckler, J. Geophys. Res. **64**, 697 (1959).
[26] E. Rieger, G. Share, D. Forrest, G. Kanbach, C. Reppin, and E. Chupp, Nature **312**, 623 (1984).
[27] E. C. Stoner and E. Wohlfarth, Phil. Trans. R. Soc. A **240**, 599 (1948).
[28] E. Thébault, C. C. Finlay, C. D. Beggan, P. Alken, J. Aubert, O. Barrois, F. Bertrand, T. Bondar, A. Boness, L. Brocco, et al., Earth, Planets Space **67**, 1 (2015).
[29] K. Levenberg, Q. Appl. Math. 2, 164 (1944).
[30] T. Williams, C. Kelley, et al. (2017), http://gnuplot.sourceforge.net/.